J. Phys. Chem. A **2009,** *113,* 4223–4241

Electronic and Vibrational Coherences in Resonance Energy Transfer along MEH-PPV Chains at Room Temperature[†]

Elisabetta Collini and Gregory D. Scholes*

Lash-Miller Chemical Laboratories, Institute for Optical Sciences and Centre for Quantum Information and Quantum Control, University of Toronto, 80 St. George Street, Toronto, Ontario M5S 3H6, Canada

Received: December 7, 2008; Revised Manuscript Received: January 22, 2009

In this work we report a study of the role of coherence dynamics in the intermediate coupling regime of electronic energy transfer (EET). Starting from the idea that in the intermediate coupling regime the phase information should be partially retained in a transfer process from a donor to an acceptor, we designed a new ultrafast experiment based on anisotropy decay along two time axes, capable of probing the degree of coherence characterizing this transfer. Conjugated polymer (poly[2-methoxy-5-(2′-ethyl-hexoxy)-1,4-phenylenevinylene], MEH-PPV) samples with different chain conformations were examined as a model multichromophoric system. The data, recorded at room temperature, reveal coherent transfer associated with intrachain energy transfer. These results were extended using two-dimensional photon echo measurements, which revealed the presence of long-lived intrachain electronic and vibrational coherences. Our results suggest that, in the intermediate coupling regime, quantum transport effects can occur when chemical bonds connecting donor and acceptor help to correlate their energy gap fluctuations. Moreover, they influence the mechanism of EET, even at room temperature.

1. Introduction

Electronic energy transfer (EET), often known as resonance energy transfer (RET), is a ubiquitous photophysical process where interchromophore interactions act to promote the transfer of excitation energy from an initially populated "donor" molecule to an "acceptor" molecule.[1] For example, electronic excitation localized on an aromatic chromophore in a polymer can migrate to nearby chromophores until it is trapped at a lower energy site.[2−6] This idea has been utilized for the design of efficient sensors.[7,8] Another example where EET plays a crucial role is the light-harvesting process in natural antenna complexes, which capture light in photosynthesis.[9−13] Understanding the mechanism of EET in these kinds of systems is important not only for a better understanding of the natural photosynthetic process but also to design new, and more efficient, devices for energy storage and conversion.[14,15] The discovery of electroluminescence[16] and photovoltaic[17] properties in conjugated polymers and their blends has prompted researchers to study EET in both dilute conjugated polymer solutions and films.[18,19] Those studies have largely focused on learning how fluorescence is quenched by trap sensitization, how emission can be tuned, and quantification of exciton diffusion lengths.

A recurring and important problem in EET theory is the discrimination between weak, intermediate, and strong electronic coupling.[20−25] In the simplest models for the fluctuating bath of nuclear motion, the mechanism of EET changes depending on the ratio between the electronic coupling U, responsible for excitonic coherence, and the dephasing constant γ, describing how the system interacts with the environment.[26] This is a closely analogous problem to the model system of two coupled states interacting with a bath[27] and general problems relating to tunneling in the condensed phase.[28] Here we report experimental studies of EET in the intermediate coupling regime. We conclude that ultrafast intrachain EET in the conjugated polymer we have studied (MEH-PPV) is a complicated nonequilibrium process involving coupled electronic and vibrational coherences. The results provide some insight into why phenylene vinylene-type conjugated polymers have semiconductor-like properties, despite the fact that chain conformational disorder is so significant.

The implications of coherence transfer in the intermediate regime can be appreciated from the microscopic point of view. When photoexcitation promotes the formation of a partially delocalized state, because of the quantum nature of this state, the excitation can be simultaneously on the donor or acceptor at any one time, as controlled by the amplitude and phase of the wave function at each site. In the dynamical evolution of the system, excitation can thereby sample simultaneously various paths for EET, thus potentially allowing control of the efficiency of the overall EET process through interference effects.[29] This mechanism contrasts with the classical hopping mechanism in which the excitation moves randomly, dissipating energy at each step and sampling just one state at any time.

The intermediate regime is particularly elusive from an experimental point of view. Coherence transfer effects expected for intermediate coupling EET, although theoretically predicted,[21,22,30−32] are difficult to detect because the very fast dephasing time present in real systems (typically 10−100 fs)[33,34] destroys coherent superposition states and precludes observation of them, particularly in the case of uncorrelated baths at the donor and acceptor sites. This is especially true at room temperature. Indirect evidence for the intermediate regime of EET has been reported by comparing measured EET dynamics with predictions from Förster theory or by considering exciton delocalization.[5,25,35−39] However, Pisliakov et al. recently predicted that the observation of electronic coherence effects in an excitonic manifold of a coupled multichromophore aggregate could be studied effectively using femtosecond two-dimensional (2D) electronic spectroscopy techniques.[40] Their prediction has

---

[†] Part of the "George C. Schatz Festschrift".

* Corresponding author, gscholes@chem.utoronto.ca.

10.1021/jp810757x CCC: $40.75

then been experimentally confirmed by 2D photon echo (2DPE) measurements on the Fenna−Matthews−Olson (FMO) photosynthetic antenna complex at 77 K.[41] In the 2D spectra, the electronic quantum coherence—a signature of intermediate coupling—is observable via quantum beating signals among different excitons, corresponding to coherent buildup and decay of populations. These recent studies have shown that ultrafast 2D electronic spectroscopy is a powerful and valuable experimental tool for examining electronic coherence effects because the method is able to discriminate coherent nuclear wavepacket motion from electronic coherence. However, it should be noted that this technique is sensitive to the effect that coherence has on the exciton population, but it does not give direct information about the dynamics of the effective coherence transfer process.

To complement the information obtained using the 2DPE technique, we recently proposed and demonstrated a new ultrafast spectroscopic experiment specifically designed to probe quantum coherent EET in the intermediate coupling case.[42] The experiment exploits the concept of anisotropy decay, and in particular its sensitivity to the dipole transition moment projection correlation function.[43] Conventional transient absorption anisotropy measurements, recorded as function of the time delay T between the pump and the probe ultrashort laser pulses, have been extensively employed to study EET in various kinds of multichromophoric systems.[44−50] Information on longer time scales after the excitation pulse have been obtained using pump−dump−probe anisotropy[51−53] and signatures in anisotropy of the strong electronic coupling limit have been proposed.[54,55] The two-time anisotropy decay (TTAD) experiment described in this work exploits the same principle. The main difference is that the anisotropy decay is recorded as a function of two different time delays (τ and T) in a three-pulse heterodyne-detected transient grating experiment. The delay T is the population time, during which excited-state dynamics such as EET occur as usual, while the delay τ, introduced between the first two pulses, scans a time period when the system is in a coherence between the ground and excited electronic states. This is the time delay scanned in photon echo experiments. In this way the experiment provides a direct probe of coherent EET processes that reorient transition dipoles during the coherence time τ.

The TTAD experiment was applied to study a prototypical conjugated polymer, poly[2-methoxy-5-(2′-ethyl-hexoxy)-1,4-phenylenevinylene] (MEH-PPV) for a number of reasons. First, EET within and among conjugated polymers has been of considerable interest, from both a practical point of view because EET is a significant source of electroluminescence quenching and a fundamental point of view since different chain conformations and packing have a non-negligible role in the mechanism of excitation evolution.[56−58] Second, conjugated polymers are good candidates for seeking intermediate coupling effects since they represent model multichromophoric systems characterized by reasonably strongly coupled chromophores (defined as the different conformational subunits in which the chain is broken).[59−68] Moreover, the fact that these subunits are randomly oriented relative to each other owing to the conformational disorder facilitates the success of anisotropy as probe for EET.

The paper is organized as follows. In section 2 we introduce and discuss the theoretical framework in which the intermediate coupling regime EET can be described. We then outline the spectroscopic signals measured with the TTAD (section 2.3) and 2DPE (section 2.4) techniques, with emphasis on the complementarity of the information attainable with the two methodologies. All the experimental details are described in section 3, whereas section 4 summarizes all the results and the discussion. In particular, section 4.1 reports the results from the preliminary characterization of the linear optical properties of the two MEH-PPV samples under study. Sections 4.2, 4.3, and 4.4 are instead dedicated to the description of the TTAD results, their modeling, and the interpretation of their oscillatory features, respectively. Particular emphasis is given to describing the results from MEH-PPV in chloroform solutions, showing evidence for coherent energy transfer, even at room temperature. The results obtained with the 2DPE technique on the same sample are illustrated in section 4.5. In section 5 we suggest a mechanism to explain our observation of coherent EET dynamics and long-lived electronic coherences detected with both TTAD and 2DPE techniques.

2. Theoretical Background

2.1. Weak and Strong Coupling Limits. In the weak coupling limit of EET, when U is much smaller than γ, the system explores the nuclear degrees of freedom faster than donor−acceptor coupling and, therefore, EET happens after complete vibrational equilibration at the photoexcited state of the donor. In this way the excitonic coherence between the donor and acceptor excited states is completely quenched by the interaction with the vibrational degrees of freedom. That means that the excitation can be on the donor or acceptor at any one time, but not on both simultaneously; therefore the EET dynamics follow classical rate laws.[1] In this situation the Förster mechanism is applicable: EET is described as an incoherent (Markovian) and irreversible hopping motion between molecules, and its rate constant is expressed as a function of the overlap integral between the emission spectrum of the donor and the absorption spectrum of the acceptor.[69] Förster initially derived the EET rate expression based on an equilibrium Fermi golden rule approach with a second-order perturbation theory treatment of the electronic coupling between donor and acceptor.[70,71] Since this original—and highly successful—formulation, much work has been done to extend the formalism of the Förster model in order to obtain a more accurate description in cases where some of the approximations fail.[72] For example, more sophisticated models have been developed to account for the coupling between transition densities beyond the point dipole description,[73−77] distance-dependent dielectric screening effects have been found,[74,75,78,79] interplay of homogeneous and inhomogeneous contributions to the spectral overlap has been examined,[11,80−82] and nonequilibrium effects have been discussed.[30]

The opposite case is the strong coupling limit, in which the donor and acceptor electronic states mix strongly to produce new, delocalized states that are little perturbed by the interaction with vibrations. Within these states, known as molecular excitons, the energy is shared quantum mechanically among several chromophores.[83] The exciton theory was first developed by Frenkel for atomic lattices[83,84] and then applied to different systems like molecular crystals[85,86] and pigment aggregates.[87,88] According to this theory, when an excitation is introduced into a system of strongly coupled monomeric units, excited-state wave functions can be constructed by taking appropriate linear combinations of the localized functions. The excited states of each monomer are then spread out in bands of levels delocalized, in the ideal case, throughout the entire system. In this situation, excitation can relax through eigenstates.[10,61,89−91] In an extended system, excitons with long coherence lengths can diffuse coherently.[92]

2.2. Intermediate Coupling Regime. In the intermediate case, when U is comparable with γ, a delocalized exciton state can still form but is considerably perturbed by the interaction with vibrations so that nonequilibrium relaxation of the bath on the time scale of EET and mixing of the donor and acceptor states leads to coherent dynamics on short time scales. This regime is possible in PPV-type conjugated polymers because the electronic coupling between conformation subunits is on the order of tens to hundreds of cm^{-1},[61] which is similar to the exciton−bath coupling.[93]

A way to think about the interplay between electronic delocalization and localization caused by bath relaxation is that excitation in a molecular aggregate is an exciton clothed by a phonon cloud. The phonon cloud lowers the system free energy by distorting the local environment around an electronically excited chromophore, whereas delocalization of excitation lowers the free energy according to the electronic coupling strength. A variational solution at any temperature can find a compromise reached between these effects.[94,95] During electronic excitation migration, the associated phonon cloud attempts to adjust. This can lead to nonequilibrium (non-Markovian) effects on ultrafast time scales as the lattice distortions are released and re-formed.[94,96]

This intermediate EET regime is of particular interest because it naturally interpolates between the classical (weak coupling, incoherent hopping mechanism) and the quantum (strong coupling, wavelike mechanism) limits. In this case the excitation can still move in space in a deterministic, classical way, but a preferred path can be chosen because the wave function is partially delocalized. Excitonic systems in which this regime applies are thus of considerable interest since, in principle, phase information can be coherently transferred through space. The intermediate coupling regime is the most challenging from the theoretical point of view since the approximations usually adopted to describe EET in the two extreme cases do not hold in this regime. So far, several theoretical studies have tried to find a unifying formalism capable of interpolating between the weak and the strong limits.[20−22,32,97−106]

Let us consider the simplest system of a two-level donor (d) and acceptor (a). The initial state where both d and a are in the ground state is indicated by $|0\rangle$, whereas $|d\rangle$ ($|a\rangle$) represents the states in which d (a) is in the excited state and a (d) in the ground state. The Hamiltonian for such a dimer can be written as

$$\mathscr{H}(t) = H - E(t)\cdot V \tag{1a}$$

$$H = H_0 + H_{\mathrm{ex}} + H_{\mathrm{ex\text{-}ph}} \tag{1b}$$

where V is the transition dipole operator, $E(t)$ is the electric field promoting transitions to excited states, and

$$H_0 = E_d|d\rangle\langle d| + E_a|a\rangle\langle a| \tag{2a}$$

$$H_{\mathrm{ex}} = U(|a\rangle\langle d| + |d\rangle\langle a|) \tag{2b}$$

$$H_{\mathrm{ex\text{-}ph}} = h_0|0\rangle\langle 0| + h_d|d\rangle\langle d| + h_a|a\rangle\langle a| \tag{2c}$$

E_d (E_a) is the energy of the state $|d\rangle$ ($|a\rangle$), U is the resonance coupling responsible for exciton formation, h_i ($i = 0, d, a$) represents the bath operator coupled to $|i\rangle$, describing the coupling of the system with vibrational degrees of freedom. The evolution of the system in time can be described by the density matrix $\rho(t)$ that at each time satisfies the Liouville equation[107,108]

$$i\hbar\frac{\mathrm{d}\rho(t)}{\mathrm{d}t} = [\mathscr{H}(t), \rho(t)] \tag{3}$$

Then, the density matrix is formally written as

$$\rho(t) = \exp_+\left\{-\frac{i}{\hbar}\int_0^t \mathscr{H}(t')\,\mathrm{d}t'\right\}|0\rangle\rho_0\langle 0|\exp_-\left\{\frac{i}{\hbar}\int_0^t \mathscr{H}(t')\,\mathrm{d}t'\right\} \tag{4}$$

where $\rho_0 = \rho(0)$ represents the initial thermal equilibrium condition. In general the probability of finding the system in the state $|d\rangle$ or $|a\rangle$, corresponding to the state population is

$$n_i(t) = Tr[\langle i|\rho(t)|i\rangle] \qquad (i = a, d) \tag{5}$$

An expression for such probability can be derived using a quantum master equation. At this point different approaches can be followed and different approximations can be applied. As opposed to the simplest approaches, in order to capture coherence effects and correctly describe the excitation transport in the intermediate coupling regime, it is important not to neglect memory (non-Markovian) effects.[23,103] These effects account for phase information transport. Accounting for non-Markovian effects is very important during short times after photoexcitation, because during this regime, correlations are established between the system and the bath.[96,109]

Following ref 32, where a generalized master equation (GME) approach was applied, the probability $n_a(t)$ can be written as

$$\frac{\mathrm{d}n_a(t)}{\mathrm{d}t} = \int_0^t dt_1 \xi_{ad}(t, t_1)[1 - n_a(t_1)] \tag{6}$$

where the memory effects are included in $\xi_{ij}(t,t_1)$, known as the electronic energy-gap correlation function and defined as[107]

$$\xi_{ad}(t, t_1) \equiv \hbar^2\langle\delta\omega_{a0}(t)\delta\omega_{d0}(t_1)\rangle \tag{7}$$

The energy gap fluctuation $\delta\omega_{i0}(t)$ is a function describing the effects of the stochastic force exerted on the system transition energies by the bath as[107]

$$\delta\omega_{i0}(t) = \frac{1}{\hbar}U_0^{\,+}(t)[h_i - h_0]U_0(t) \tag{8}$$

where $U_0(t) = \exp\{-ih_0t/\hbar\}$ is the ground-state evolution operator. When $i = j$, a "diagonal" correlation function is obtained, which correlates the energy gap function with itself. This quantity has a classical analogue and it can be related to the spectral density by a Fourier transform.[107] The cross correlation functions ($i \neq j$), which have no classical analogue, are key quantities for understanding the effects of coherence in EET. When $\xi_{ad} = 0$, according to eq 7, the fluctuations of the transition energies ω_{d0} and ω_{a0} are uncorrelated, and coherent EET cannot contribute to the overall transfer process unless the electronic coupling is strong.[110] This is the usual assumption in theories for EET. The observation of coherent effects is connected with a nonvanishing value of ξ_{ad}.

When the bath correlation function is approximated as exponentially relaxing, and the high temperature limit is assumed, then we can define γ as the dephasing strength, proportional to the inverse of the decoherence time τ_c. Then, using eq 6, it is possible define more clearly the two limiting regimes of EET (Figure 1). When $U \gg \gamma$ (strong coupling) and the time difference $t - t_1$ is much smaller than the lifetime $\tau_c = \hbar/\gamma$ of the memory function, $\xi_{ij}(t,t_1)$ becomes time independent and the persistent memory produces a pure exciton where the probability n_a oscillates indefinitely according to (Figure 1a)

$$n_a(t) \approx \sin^2(Ut/\hbar) \tag{9}$$

On the other hand, if $U \ll \gamma$ and $t - t_1$ is much bigger than τ_c, EET takes place in the weak limit regime. In this situation, the Markovian approximation holds and the generalized master equation converges to a Pauli master equation (Figure 1c)

$$n_a(t) \approx \frac{1}{2}\left[1 - \exp\left(-\frac{4U^2}{\gamma\hbar}\right)\right] \tag{10}$$

In the intermediate case Kimura et al. derive[32]

$$n_a(t) = \frac{1}{2}\left[1 - e^{-\gamma t/2\hbar}\left\{\cosh(\sqrt{\alpha}t) + \frac{\gamma}{2\hbar\sqrt{\alpha}}\sinh(\sqrt{\alpha}t)\right\}\right] \tag{11a}$$

for $U > \gamma/4$

$$n_a(t) = \frac{1}{2}\left[1 - e^{-\gamma t/2\hbar}\left\{\cos(\sqrt{|\alpha|}t) + \frac{\gamma}{2\hbar\sqrt{|\alpha|}}\sin(\sqrt{|\alpha|}t)\right\}\right] \tag{11b}$$

for $U < \gamma/4$, where

$$\alpha \equiv \frac{\gamma^2}{4\hbar^2} - \frac{4U^2}{\hbar^2} \tag{12}$$

According to eqs 11, EET in the intermediate case can take place by two kinds of mechanisms. In the first case, eq 11a, EET happens while retaining the oscillatory coherent character, until it is quenched owing to bath perturbations. In this condition n_a shows a characteristic damped oscillating behavior, Figure 1b. In the second case eq 11b, no oscillations are recorded, but the EET takes place quickly, simultaneously with the vibrational relaxation. This is an example of nonequilibrum EET.[30] The experimental challenge of investigating EET dynamics in these regimes is the focus of this paper.

2.3. Two-Time Anisotropy Decay. In a conventional transient absorption anisotropy experiment the components of the signal polarized parallel and perpendicular to the polarization of the exciting pulse are recorded as a function of the delay between the pump and the probe ultrashort laser pulses, T. The anisotropy decay as a function of T is then retrieved as the difference between the two components, normalized by the total intensity decay. The time profile of that decay provides information about transition dipole moment reorientation during the excited-state lifetime. Thus time-resolved anisotropy has been extensively exploited to study EET in various kinds of multichromophoric systems.[6,45,49,111−120]

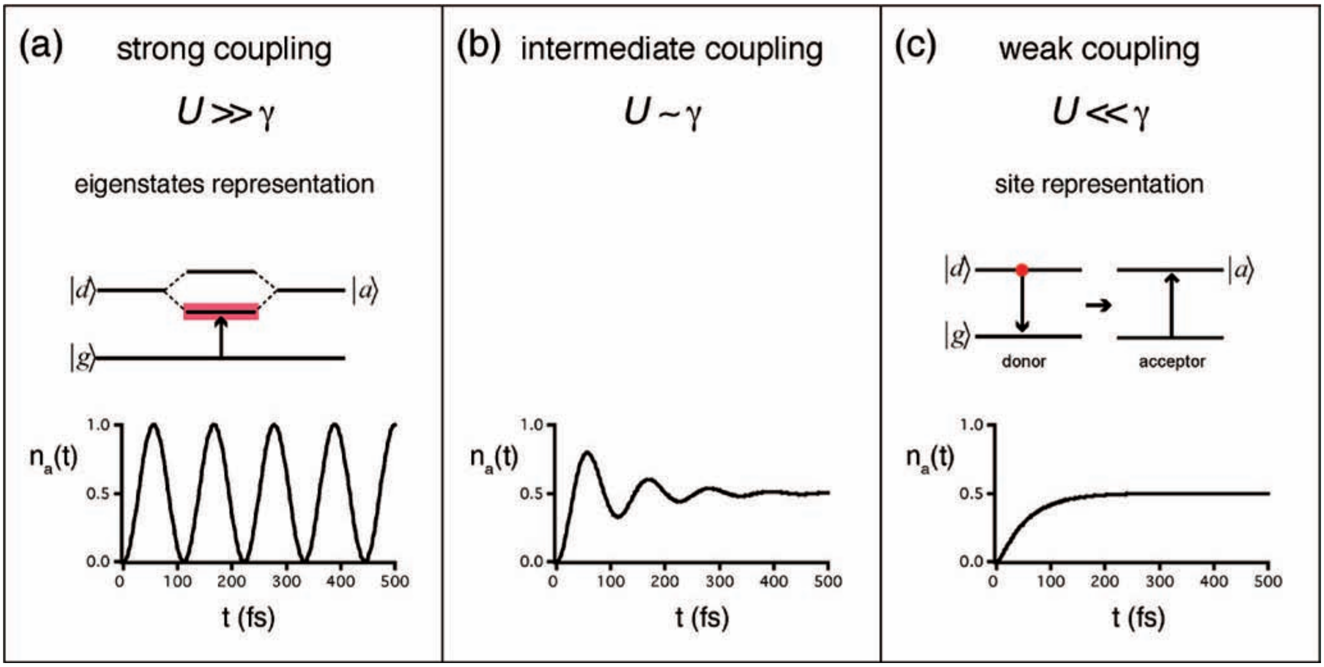

Figure 1. Comparison between different regimes of EET. The probability to find the excitation on the acceptor state $n_a(t)$ is calculated using eqs 11 with γ fixed at 150 cm^{-1} and $U = 0$, 100, and 1000 cm^{-1} for (a), (b), and (c), respectively. In the strong coupling limit (a), the electronic state of the donor and the acceptor mix strongly to produce a new delocalized state (exciton). Within this state the excitation energy is shared quantum mechanically between the donor and the acceptor excited states (red highlighted area) and the probability to find the excitation on the acceptor state $n_a(t)$ is an oscillating function with period depending on the electronic coupling U. In the weak coupling limit (c), the excitation energy is transferred incoherently and irreversibly between different sites. The probability $n_a(t)$ is an exponential function of t. In the intermediate coupling limit (b) the excitation moves in space, yet part of the phase information is conserved (coherence effect). $n_a(t)$ shows a damped oscillatory behavior depending on the relative magnitudes of the electronic coupling U and the decoherence time τ_c.

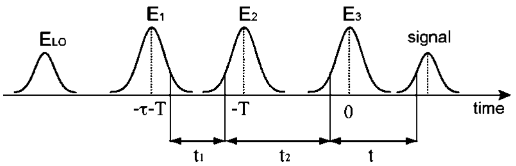

Figure 2. General four-wave mixing pulse sequence and definition of time variables. The delays τ and T, conventionally called coherence and population time, respectively, are defined as the delay between the centers of pulse pairs (E_1, E_2) and (E_2, E_3), respectively. To account for finite pulse duration, we introduce t_1 and t_2 as the delays between the field-matter interaction points. In the limit of short pulses $t_1 = \tau$ and $t_2 = T$, t is the signal evolution time defined relative to the third pulse.

To study coherent energy transfer directly, a new ultrafast experiment, called two-time anisotropy decay (TTAD), was specifically designed.[42] The principle is to measure the anisotropy decay not only as a function of T, like in the conventional anisotropy decay experiments, but also as a function of τ in a three-pulse heterodyne detected transient grating experiment (see Figure 2 for the definition of the time variables). In this section the theoretical background of the different EET regimes previously outlined will first be reviewed to motivate why this technique is sensitive to coherence transfer in the intermediate coupling EET regime.

Equations 1−5 show that the evolution of the probability density is determined by the forward ($|d\rangle$ to $|a\rangle$) and reverse propagation of the system as dictated by the Hamiltonian of the system. Throughout each of these paths, the states $|d\rangle$ and $|a\rangle$ (i) can couple directly to each other via H_{ex} (eq 2b) and be involved in the formation of an excitonic state or (ii) they can interact with the nuclear degrees of freedom through $H_{\mathrm{ex\text{-}ph}}$ (eq 2c). Note that, while H_{ex} contributes to exciton formation, $H_{\mathrm{ex\text{-}ph}}$ is instead responsible for their disruption (localization of excitation). From this point of view, it can be asserted that the intermediate regime, when these two Hamiltonians have comparable weight, is characterized by a competition between the formation of eigenstates and their destruction, caused by coupling to bath fluctuations. Moreover, since in this regime excitons can still be formed, phase information should be retained in the $|d\rangle$ to $|a\rangle$ propagation when excitation is transferred.

In experiments like pump−probe and conventional anisotropy, the first two field−matter interactions happen simultaneously ($\tau = 0$), directly creating a population. The probe pulse also detects only populations. Since the phase information is lost when populations are formed, these techniques are sensitive only to probability density, and therefore coherence effects connected with phase conservation cannot be captured. For this reason we "added" to the conventional anisotropy experiment another time axis τ, which is the time delay conventionally scanned in a photon echo experiment. In this way we are able to follow the evolution of the coherence formed after the interaction with the first field. By measuring dynamics in the first coherence time period τ and using anisotropy to quantitatively follow the transfer of excitation coherence, we probe the memory, or degree of coherence, characteristic of the $|d\rangle$ to $|a\rangle$ forward propagation. Whether or not this process occurs is important to establish because it is often neglected in theory by making the secular approximation.

In order to validate the results of this new experiment, it is important to demonstrate that the anisotropy expression is still meaningful for a scan over the coherence time τ and in the case of small T delays, when pulses are overlapped. This can be shown by summarizing the derivation of the anisotropy decay as a function of τ and T. Starting from the conventional form of anisotropy decay[43]

$$r(\tau, T) = \frac{S_{\|}(\tau, T) - S_{\perp}(\tau, T)}{S_{\|}(\tau, T) + 2S_{\perp}(\tau, T)} \tag{13}$$

where $S_{\|}$ and $S_{\perp}$ are the third-order nonlinear signals measured with the probe pulse electric field E_3 polarized parallel and perpendicular to the polarization of the exciting pulse sequence (E_1 and E_2), respectively.

In general, the change in signal intensity as a function of pulse delays in a heterodyne detected experiment can be expressed as

$$S(t_1, t_2) \propto \int_0^{\infty} \mathrm{d}t \{E_{\mathrm{LO}}^{*} \langle P^{(3)}(t_1, t_2, t\rangle \, \mathrm{e}^{\mathrm{i}\phi}\} \tag{14}$$

where E_{LO} is the electric field of the local oscillator (LO), ϕ is the relative phase between the LO and the signal field, asterisk indicates the complex conjugate, and t_1 and t_2 are the time delays between pulses 1 and 2 and between 2 and 3 as illustrated in Figure 2, respectively. The key quantity to determine any four-wave mixing nonlinear signal is third-order polarization $P^{(3)}$ which can be expressed as the convolution of the nonlinear response function $\mathscr{R}^{(3)}(t_1,t_2,t)$ with the field envelopes

$$P^{(3)}(t_1, t_2, t) \propto \int_0^{\infty} \mathrm{d}t \int_0^{\infty} \mathrm{d}t_2 \int_0^{\infty} \mathrm{d}t_1 \mathscr{R}^{(3)}(t_1, t_2, t) \mathbf{E}_1^{*}(\mathbf{k}_1, t_1) \mathbf{E}_2(\mathbf{k}_2, t_2) \mathbf{E}_3(\mathbf{k}_3, t) \tag{15}$$

In the impulsive limit $\mathscr{R}^{(3)}(t_1,t_2,t)$ can be written as

$$\mathscr{R}^{(3)}(t, t_2, t_1) = \left(\frac{i}{\hbar}\right)^3 \langle [[[V(t + t_2 + t_1), V(t_2 + t_1)], V(t_1)], V(0)]\rho_0\rangle \tag{16}$$

where the time dependence of the dipole operator V is determined by solving the Heisenberg equation of motion. The expansion of the three commutators in eq 16 separates naturally into several contributions R_{α}, each representing a different time ordering of the various interactions.[107] These different contributions are called Liouville space pathways and are usually graphically visualized by means of double-sided Feynman diagrams. The nonlinear response function is then calculated by summing over the various possible pathways R_{α} in Liouville space, which contribute to the induced optical polarization

$$\mathscr{R}^{(3)}(t_1, t_2, t) = \sum_{\alpha} C_{\alpha}^{(4)} R_{\alpha}(t_1, t_2, t) \tag{17}$$

$C_{\alpha}^{(4)}$ relates the laboratory frame pump and probe pulse polarizations to the dipole transition moments of the molecules being photoexcited, allowing rotational averaging the response function with respect to the field polarizations.[6,45,115,121−123] It has been demonstrated that for randomly oriented molecules this relationship between laboratory and molecular frames is governed by an isotropic Cartesian tensor.[124,125] It is derived in section 4.3.

If the finite pulse duration of the fields is taken into account, the integrations over the finite pulse durations in eq 14 have to be carried out in such a manner that response functions accounting for non-time-ordered pulse sequences are correctly accounted for (e.g., to reproduce the coherent spike).[126] That summation, which is over t_1 and t_2, is done by a coarse graining procedure, meaning that in the limit of short pulses compared to τ and T, we have $t_1 = \tau$ and $t_2 = T$. This is a standard procedure, see for example ref 126.

It is interesting to note that the anisotropy decay can be retrieved even when τ and/or T are smaller than the pulse duration because the sum over response functions cancels in eq 13, except for the factor that gives the time dependence of the ensemble averaged transition dipole randomization.[61] In the case where only ground-state bleach and stimulated emission dominate the signal, the cancelation is exact. When excited-state absorption is significant, the expression needs to be considered case by case.[127] Hence, for instance, the coherent spike (nontime ordered response function during pulse overlap) often has little effect on the anisotropy because it is removed by the ratio of signal intensities. Therefore it is possible to define anisotropy quantitatively (a) during pulse overlap and (b) as a function of either τ or T, provided that pulse ordering and finite pulse durations are accounted for together with their influence on the Feynman diagrams that generate signals. The effect of polarization on each relevant Feynman diagram also needs to be ascertained (vide infra).

2.4. 2D Photon Echo. Electronic two-dimensional photon echo (2DPE) spectroscopy is a four-wave mixing experiment in which a sequence of three ultrashort laser fields and a strongly attenuated local oscillator interact with the sample to create a polarization that radiates into the phase matched direction $\mathbf{k}_s = -\mathbf{k}_1 + \mathbf{k}_2 + \mathbf{k}_3$.[128] The full electric field of the signal is heterodyne-detected using spectral interferometry while the delay T between the second and the third pulse is fixed and the delay τ between the first and the second pulse is varied. After Fourier transform with respect to τ and the rephasing time t (defined as the time delay between the third pulse and the signal), the 2D electronic spectrum at a given population time T can be retrieved.[129,130] The final result is a 2D map in which the signal amplitude (real, imaginary or absolute value) is plotted as a function of the coherence frequency ω_τ, representing the initial excitation, and of the rephasing frequency ω_t, which can be interpreted as the ensuing emission.[128] 2D spectroscopy has been reviewed recently in detail, both from the experimental and theoretical points of view.[128,131] In this section the basic formalism that will be used in later sections is briefly described.

The total 2D Fourier-transformed spectrum is given by a double Fourier transform of the photon echo polarization field $P^{(3)}(\tau,T,t)$with respect to τ and t

$$S_{2D} \approx \int_{-\infty}^{\infty} d\tau \int_{-\infty}^{\infty} dt\, e^{-i\omega_\tau \tau} e^{i\omega_t t}\, iP^{(3)}(\tau, T, t) \qquad (18)$$

Note that the 2D signal is a complex quantity but in the next sections only the real part, which is associated with the absorptive signal contribution, will be considered. In the common perturbative approach, $P^{(3)}(\tau,T,t)$ is described as a linear combination of response functions (cf. previous section).[107] This approach has been extensively applied to model the main features in the 2D spectra of coupled systems, allowing the elucidation of electronic couplings, energy transfer dynamics, solvation dynamics, and solute−solvent interactions.[40,132−136]

Recently a nonperturbative method was proposed to model $P^{(3)}(\tau,T,t)$ for 2D data simulations.[40,103,133,137] The authors combined a time-nonlocal quantum master equation formalism[138] with a recently developed reduced density matrix description incorporating the relevant laser pulses into the system Hamiltonian.[139] Effects of coherent energy transfer and non-Markovian dynamics were included in the model. Simulations performed with this approach evidenced two groups of processes with different dependences on T. Together with the conventional population dynamics, processes like ground-state bleaching (GSB), stimulated emission (SE), and excited-state absorption (ESA),[140] a periodic behavior connected with electronic coherence, were also discovered. It was found to appear as a shape and intensity modulation of cross and diagonal peaks (quantum beats).[133,137]

To appreciate the difference between these two kinds of contribution, a convenient and intuitive way is to look at the Feynman diagrams. In general, because of the broad bandwidth associated with a femtosecond laser pulse, the first field−matter interaction generates a coherent superposition of multiple vibronic coherences between ground state and excited states. Then, if the second interaction generates an exciton population state (diagonal density matrix elements $\rho_{00}^{(2)}$ or $\rho_{ii}^{(2)}$), GSB, SE, and ESA are accounted for. These diagrams (not shown) give rise to nonoscillating contributions, positive for GSB and SE and negative for ESA both along the diagonal and in off-diagonal positions. The intensity of each of these contributions is determined by the system parameters, in particular, by a product of dipole transition moments. The second light−matter interaction could, instead, generate an electronic coherence (off-diagonal density matrix elements, $\rho_{ij,i\neq j}^{(2)}$). The time evolution of such a signal contribution has an oscillating phase factor with frequency equal to the energy difference between the pair of coupled excited states i and j. Therefore, these contributions can be seen as excitonic quantum beats in the 2D spectra. The Feynman diagrams accounting for this contribution are shown in Figure 3. Notice that diagrams a and b, responsible for beats in cross-peaks, have a rephasing pulse sequence ($\tau > 0$) while diagrams c and d, causing the modulation in the diagonal peaks, are nonrephasing ($\tau < 0$). This explains why diagonal peaks exhibit an oscillatory behavior with the same modulation period but much smaller amplitude than cross peaks.[137]

An important point that can be stressed by looking at the diagrams is that 2DPE is sensitive to coherence effects during T, and therefore it measures the coherent buildup and decay of population. However this technique is not an incisive probe of coherence transfer, that is the coherent EET during τ from $|0\rangle\langle d|$ to $|0\rangle\langle a|$. To examine that process, we use TTAD.

3. Experimental Methods

The laser system used in this work has been described in detail previously.[141] Pulses from a Ti:sapphire regeneratively amplified Clark-MXR CPA-2001 laser system (1 kHz, 775 nm, 140 fs pulses) were converted into visible light by means of a noncollinear optical parametric amplifier (NOPA) and then recompressed by a pair of quartz prisms. All measurements were performed with the central wavelength of the NOPA set to 527 nm.

The experimental setup (Figure 4) is similar to that for conventional optical heterodyne detected transient grating (OHD-TG) spectroscopy, described in refs 142 and 143. After prism compression, the pulse from the NOPA was split by a 50% beam splitter, and one beam was delayed using a retroreflector mounted on a computer-controlled motorized

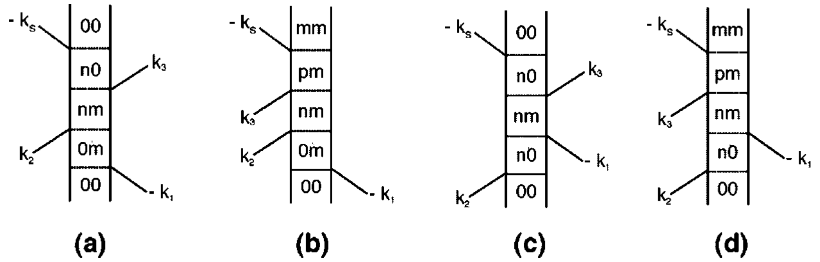

Figure 3. Double-sided Feynman diagrams for the nonlinear third-order polarization in the $-\mathbf{k}_1 + \mathbf{k}_2 + \mathbf{k}_3$ phase matching direction in the impulsive limit accounting for the coherence dynamics in 2D photon echo. In these diagrams, $|0\rangle$ denotes the ground state, $|m\rangle$, $|n\rangle$ denote one-exciton states, and $|p\rangle$ represents a two-exciton state. In all the four pathways, the system is prepared in a coherence state $|n\rangle\langle m|$ during the population time T; therefore, an oscillating phase factor with a frequency ΔE_{nm} is associated with these terms. Diagrams a and b are rephasing diagrams ($\tau > 0$) that contribute to the cross peak, whereas (c) and (d) are nonrephasing diagrams ($\tau < 0$) that contribute to the diagonal peak.

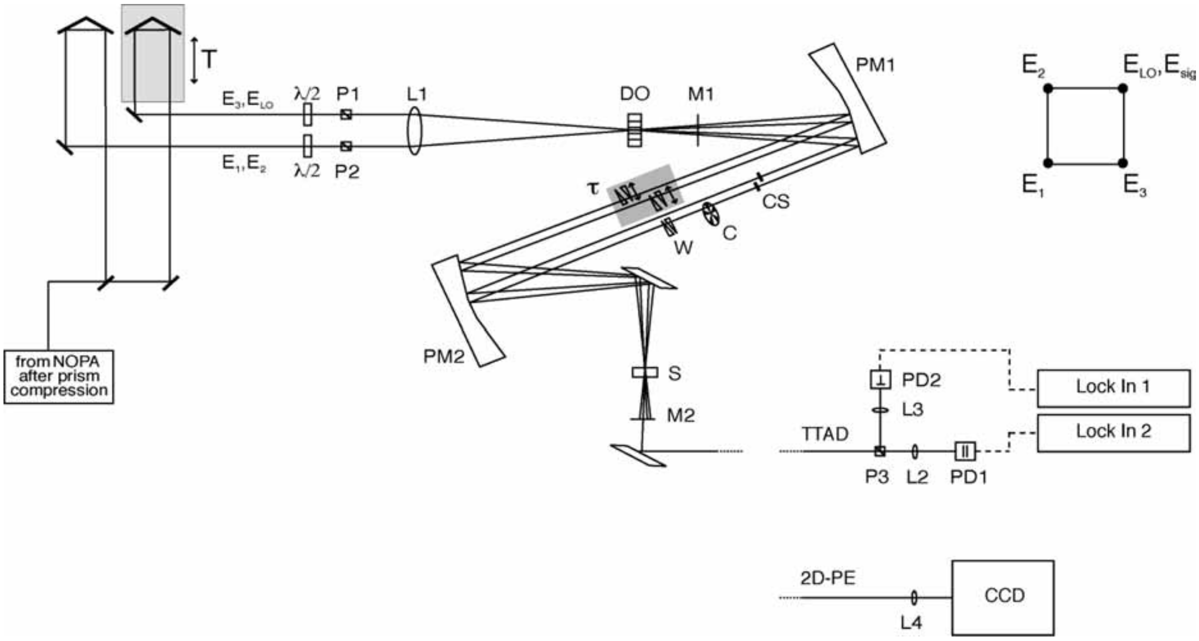

Figure 4. Experimental setup for the two-time anisotropy decay (TTAD) and 2D photon echo (2DPE) experiments. Apart from the coverslips (CS) used in the TTAD, but removed for the 2DPE experiment, the two setups differ only in the apparatus after the sample position. $\lambda/2$: half-waveplate, P_i, polarizer cube; G, glass plate; L_i, lens; DO, diffractive optic; M_i, mask; PM_i, parabolic mirror; CS, coverslip; C, chopper; W, glass wedges; S, sample; PD_i, photodiode. In the inset, the boxcar geometry of the four beams in front of the sample is shown (E_1, E_2, pump pulses; E_3, probe pulse; E_{LO}, local oscillator). The signal field ($\mathbf{k}_s = -\mathbf{k}_1 + \mathbf{k}_2 + \mathbf{k}_3$) is radiated along the same direction as the local oscillator ($\mathbf{k}_{LO}$), and it is spatially and temporally overlapped with it.

translation stage to set the delay time T. The relative intensity of the two beams was controlled by a combination of a half-plate and polarizer ($\lambda/2$, P1, P2) inserted in each optical path.

Following the experimental arrangement commonly used for passively phase-locked OHD-TG,[143,144] the two beams were then spatially overlapped on a diffractive optic (DO) with a 10 cm focal length achromatic lens (L1). The DO splits each beam into two replicas (±1 diffractive orders) with an efficiency of 70%, while all other diffraction orders are blocked by a spatial filter (M1). This provides four diffracted beams in a boxcar geometry: two probe pulses (E_1, E_2) propagating in the $\mathbf{k}_1$ and $\mathbf{k}_2$ directions, respectively, a probe pulse (E_3) in the $\mathbf{k}_3$ direction, and a local oscillator in the $\mathbf{k}_{LO}$ direction. These four beams were achromatically collimated and focused into the sample (S) by a pair of 10 cm focal length parabolic mirrors (PM1, PM2).

An additional delay time (τ) between the two pump pulses was introduced by means of movable glass wedge pairs (W) inserted in both E_1 and E_2 pathways following the method proposed by Brixner et al. in refs 145 and 146. One of the wedges in each pair was mounted on a motorized translation stage. Translation of one wedge with respect to the other changes the material path length traversed by the pulse without changing the alignment, thus varying the pulse arrival time at the sample.

The instrument response function was determined by exploiting optical Kerr effect (OKE) measurements on pure solvents, estimating a pulse duration (full width at half-maximum, fwhm) of 30 fs. Moreover, the time−bandwidth product, obtained multiplying this value by the spectral bandwidth (measured to be 500 cm^{-1}) is 0.45, in good agreement with the theoretical value of 0.441 for an ideal transform-limited Gaussian pulse.

In the two-time anisotropy decay (TTAD) experiment, a given coherence time τ was set by choosing a suitable position of the movable wedge in E_1, while the population time T was scanned. According to the boxcar geometry phase matching condition, the signal field propagates in the same direction as the LO (Figure 4), leading to a spectral interference pattern depending on the relative phase between them. It was then possible to measure separately the imaginary or the real part of the signal by choosing the phase of the LO in quadrature or in phase with the signal field, respectively. Two identical microscope coverslips (CS) were inserted into E_3 and E_{LO} paths, and the CS in the LO path was mounted on a motor-driven rotation stage to control the phase difference between the LO and the signal fields. To avoid any contribution from unwanted pump−probe signal due to the LO and the two pump pulses, the probe beam was chopped at 342 Hz before the sample. Any contamination due to a homodyne signal was removed by subtracting the two independently measured signals phase shifted by π.

To calculate anisotropy, strict control of the polarization of the beams is required. To this aim, the two polarizers P1 and P2 inserted prior to the diffractive optic were oriented so that the polarization of the two pump pulses E_1 and E_2 was vertical, whereas the polarization of the probe pulse and the LO was at 45° relative to the vertical. This allowed simultaneous recording of the components of the signal polarized parallel ($S_{\|}$) and perpendicular ($S_{\perp}$) to the polarization of the exciting pulses. The two components were split after the sample by means of a cube polarizer (P3) and detected by two silicon photodiodes (PD1, PD2) and two lock-in amplifiers.

The OKE effect was also employed to calibrate the phase between the probe and LO beams, i.e., to find the relative position of the CS corresponding to the two fields in quadrature or in phase. To this aim, the signal of the pure solvent at $T = \tau = 0$ was measured while varying the relative angle between the two CS. For nonresonant systems, such as transparent solvents, the contribution of the real part of the third-order polarization, connected to the OKE, is much larger than the corresponding imaginary part (the dichroic signal is nearly zero). Hence the relative phase for measuring imaginary and real components correspond to the CS position at which the signal is zero and maximum, respectively. The phase stability was checked during the day, and a phase drift of about 5° was recorded after 24 h.

The E_1-E_2 delay calibration was performed using a similar methodology. The calibration procedure suggested by Brixner et al.[145,146] requires replacing the sample with a second DO, identical to the first one, so that E_1 and E_2 pulses are diffracted into one common direction leading to a spectral interference pattern. In the present work we used a different method. We scanned the E_1-E_2 delay at a suboptical period step size while detecting the heterodyned FWM signal for a solvent (typically CCl_4). The signal phase cycles as the delay is scanned; the number of phase oscillations per unit of wedge displacement can be easily converted into number of oscillations per femtosecond through the frequency value.

2D photon echo (2DPE) measurements were performed with the same setup used for the TTAD but with a different signal detection apparatus, as shown in Figure 4. Contrary to the TTAD acquisition scheme, in the 2DPE experiment for any given population time T, the coherence time τ was scanned moving the wedge in E_1 from $-(\tau + T)$ to $-T$ and then the wedge in E_2 from $-T$ to $-(\tau + T)$ with a typical time step of 0.5 fs. Also in this case, the boxcar geometry guarantees the copropagation of the signal field with the LO. The resulting interference intensity was focused into a 0.63 m spectrograph (25 μm slit) and recorded using a 16 bit, 400 × 1600 pixel, thermoelectrically cooled charge-coupled device detector (CCD). At each value of τ a different spectrum was obtained and stored in a 2D matrix from which the desired spectral signal intensity and phase were retrieved through a Fourier-transform evaluation method, as described elsewhere.[129,130,147−149]

Unwanted scattering contributions due to the interference of the LO with the two pump pulses (E_1, E_2) were automatically subtracted from the recorded signal at each τ value by means of a chopper (4.5 Hz) inserted in the E_3 path. Before Fourier analysis the signal was also corrected for the contribution of scattering from E_3 by subtracting the E_3-E_{LO} interference spectrum recorded at the beginning of the experiment.[145]

As opposed to the TTAD experiment, in which the phase between the signal and the LO is decided a priori by setting the position of the CS so only the imaginary or real part of the signal is eventually detected, in the 2DPE the total interference intensity is sent to the detector and the real and imaginary parts were retrieved by later data analysis. For an accurate calibration of the absolute phase of the signal, spectrally resolved pump−probe data for the sample were separately recorded. These data can be related to the real (absorptive) part of the projection of the 2D spectrum along the ω_t axis according to the projection-slice theorem.[129,130]

Each 2D trace is the average of three separate scans. At the end of each series of 2D scans at different T, a scan at the first T value is repeated to check the long time reproducibility. The decrease of the absolute value of the 2D signal was on average less than 20%, and the qualitative shape of the signal did not change within the experimental noise. Each series of 2D scans at different T was further repeated several times on different days for comparison. To ensure that the LO did not influence the response of the system, its intensity was attenuated by about 3 orders of magnitude relative to the other beams and the time ordering was set so that the LO always preceded the probe by ~500 fs.

Poly[2-methoxy-5-(2′-ethyl-hexoxy)-1,4-phenylenevinylene] (MEH-PPV, MW 150000 g/mol) was purchased from American Dye Source, Inc., and used as received. Solutions of MEH-PPV in chloroform, as well as aqueous suspensions of polymer nanoparticles,[150] were prepared and filtered to remove insoluble impurities. The optical density (OD) of each solution was adjusted to be about 0.3 in a 100 μm path length cell.

To minimize artifacts caused by sample degradation, in both experiments the pulse energy was kept at less than 5 nJ/pulse and the solution was circulated through a 100 μm path length cell from a reservoir containing ~15 mL of solution. To ensure that the sample had not photodegraded during the measurements, the absorption spectrum of the sample was collected before and after each measurement. All of the measurements were performed at room temperature (20 ± 1 °C). In the TTAD measurements, the effects of exciton−exciton annihilation, which introduce a fast anisotropy decay component, were minimized by reducing the incident laser intensity until the decay profiles showed no change with further intensity reduction. The laser fluence was estimated to be <100 μJ/cm^2.

4. Results and Discussion

4.1. Photophysics of MEH-PPV. Conjugated polymers are molecules characterized by extensive π-electron conjugation along a rigid backbone. Thus, in perfectly ordered polymer chains, wave functions can have extraordinary coherence lengths at low temperature.[151] In solution, however, the chains adopt various conformations owing to the relatively low energy barrier for small angle rotations around bonds along the backbone.[152,153] The twisting of the main chain randomly introduces physical defects along the conjugated backbone, inhibiting the delocalization of π-electrons throughout the entire polymeric molecule. Therefore, isolated chains of MEH-PPV in solution can be considered as an ensemble of quasi-localized chromophores, with various conjugation lengths.[62−68,154−156] The average conjugation length is about seven repeat units.[61] These individual conformational subunits, or chromophores, absorb light at different wavelengths yielding a broad absorption band.

The concept of conformational subunits with respect to torsional disorder is somewhat vague since the definition of a break in the conjugation is subjective,[59,157] and entropic considerations likely play a role in determining effective conjugation length.[158,159] Recent work has further suggested that the description in terms of an ensemble of quasi-localized chromophores is not generally applicable to all classes of conjugated polymers.[157,160] However, extensive theoretical and experimental studies have shown that such a description is meaningful for polymers in the PPV family. It is then reasonable to describe the MEH-PPV chain as an ensemble of subunits electronically coupled to each other.[61,161] Each subunit is intimately connected to the neighboring ones by the σ-bond framework of the polymer chain, so the coupling between them has been found to be reasonably strong.[162] This leads to the formation of subtly delocalized collective states of nanoscale excitons that influence the polymer optical properties.[59,93,117,118,163] Conjugated polymer conformation determines the nature of the interaction and the coupling between different subunits, which in turn decides how energy is transported along the chain.[164−166]

Two basic types of EET have been identified: intrachain and interchain.[155,162,167−169] The former consists of energy migration along the backbone between adjacent segments. The latter can be described as energy hopping among segments coupled through space either because the chains are near to each other in a solid film or because the chain is folded back on itself. The intrachain transfer is generally the predominant mechanism when the polymer chain assumes an open, extended conformation, such as in a good solvent. On the other hand, interchain interactions predominate in a tightly coiled configuration, as in nanoparticle suspensions or solid films.[164,170] Moreover, quantum chemical simulations have demonstrated that interchain EET is more efficient than intrachain EET, due to the larger electronic coupling between cofacial conformational subunits compared to those in a linear arrangement.[162]

If EET occurs solely by the Förster mechanism, this would imply that conformational subunits are uncoupled chromophores, i.e., the exciton coherence length is the same as the conformational subunit size.[161] Such a conclusion is inconsistent with the interpretation of 3PEPS (three-pulse photon echo peak shift) data.[161,163,171] To examine whether electronic coherence is longer than individual conformational subunits, we compare samples characterized by polymer chains in two different limiting conformations: (i) solutions in a good solvent allowing an open chain configuration and (ii) aqueous suspensions of polymer nanoparticles (NP) formed by individual collapsed chains. Previous spectroscopic and morphological characterization of suspended NPs revealed a reduction in the mean conjugation length associated with bending or kinking of the polymer backbone as well as efficient interchain EET.[150,172] Conjugated polymer NPs have gained interest as fluorescence probes in imaging and biosensing and as useful model systems for studying EET in dense, nanostructured, multichromophoric systems.[173−175]

Figure 5 shows the room-temperature absorption and photoluminescence spectra of a MEH-PPV solution in chloroform (CF) and an aqueous suspension of MEH-PPV NPs. The spectra of both samples exhibit typical features of this class of conjugated polymer: a broad, unstructured absorption band and a narrower, vibronically structured fluorescence. Isolated chains of MEH-PPV dissolved in CF exhibit an absorption spectrum centered around 495 nm. The NPs dispersed in water manifest broadened absorption and red-shifted fluorescence spectra compared to those of the polymer in CF solution. The blue-shifted contribution to the absorption band is consistent with a small overall decrease in the conjugation length, attributable to the bending or kinking of the polymer backbone.[176,177] A red tail is also evident in the absorption spectrum of NPs, indicating the presence of aggregate states formed by interactions between segments of the polymer chain.[178,179] On the other hand, in good solvents like CF, the individual polymer chains are expected to assume a relatively open and straight conformation, which maximizes favorable solute−solvent interactions,[177,180] as recently shown by theoretical studies.[165]

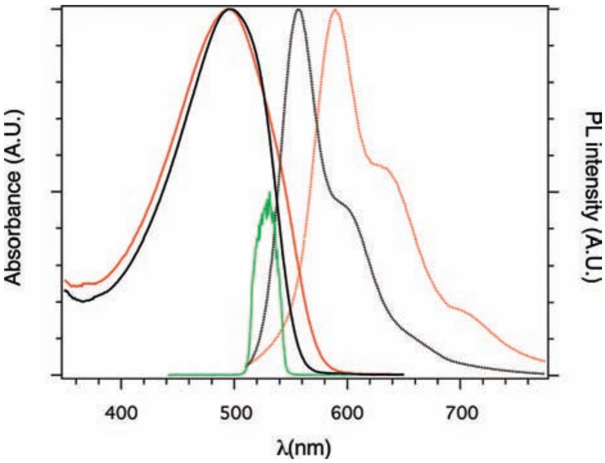

Figure 5. Normalized absorption (solid lines) and photoluminescence (dotted lines) spectra of MEH-PPV solution in chloroform (black) and of MEH-PPV nanoparticles suspension in water (red). The spectral profile of the exciting pulse is also reported (green).

Similarly to film samples, the fluorescence spectrum of the NP suspension is red-shifted and shows a large Stokes shift, attributed to energy transfer to low-energy chromophores and weakly fluorescent aggregates.[181,182] The fluorescence yield of the aqueous suspension is also reduced compared to that of the CF solution, in agreement with reports of decreased, red-shifted fluorescence of MEH-PPV in solvent mixtures containing the poor solvent methanol.[181] The fluorescence quenching is attributed to energy transfer to weakly fluorescent intrachain aggregates.

4.2. TTAD Results. The TTAD data for the CF solution and NP suspension are plotted in Figure 6. All these data are the average of 9−10 repeated measurements. In order to rule out any possible experimental artifacts affecting the anisotropy along the τ axis and to check the polarization control of the incoming beams, the experiment was at first tested with a laser dye that absorbs in the same spectral region of MEH-PPV, Rhodamine 6G dissolved in ethanol. The solution is sufficiently dilute that no interchromophore EET can occur during the time scale of the experiment. The experimental data recorded at different T and τ values over the range confirmed that the recorded initial anisotropy corresponds, within the experimental error, to the expected theoretical value of 0.4. No dependence on the τ axis delay was detected.

In Figure 6, experimental data recorded for MEH-PPV in a CF solution (upper panels) and a MEH-PPV NPs suspension (lower panels) are compared; in parts a and b of Figure 6, the 3D plots showing the TTAD surface as a function of both T and τ are reported, whereas in panels c and d of Figure 6 and panels e and f are slices through the experimental surface along the T or τ axis are displayed, respectively. To allow a better comparison, in panels b and e only biexponential fits to the data are shown.

Let us focus at first on panels b and e, representing the decays of anisotropy along T. All the anisotropy decays as a function of T were fit with two exponentials and a static offset. The fitting

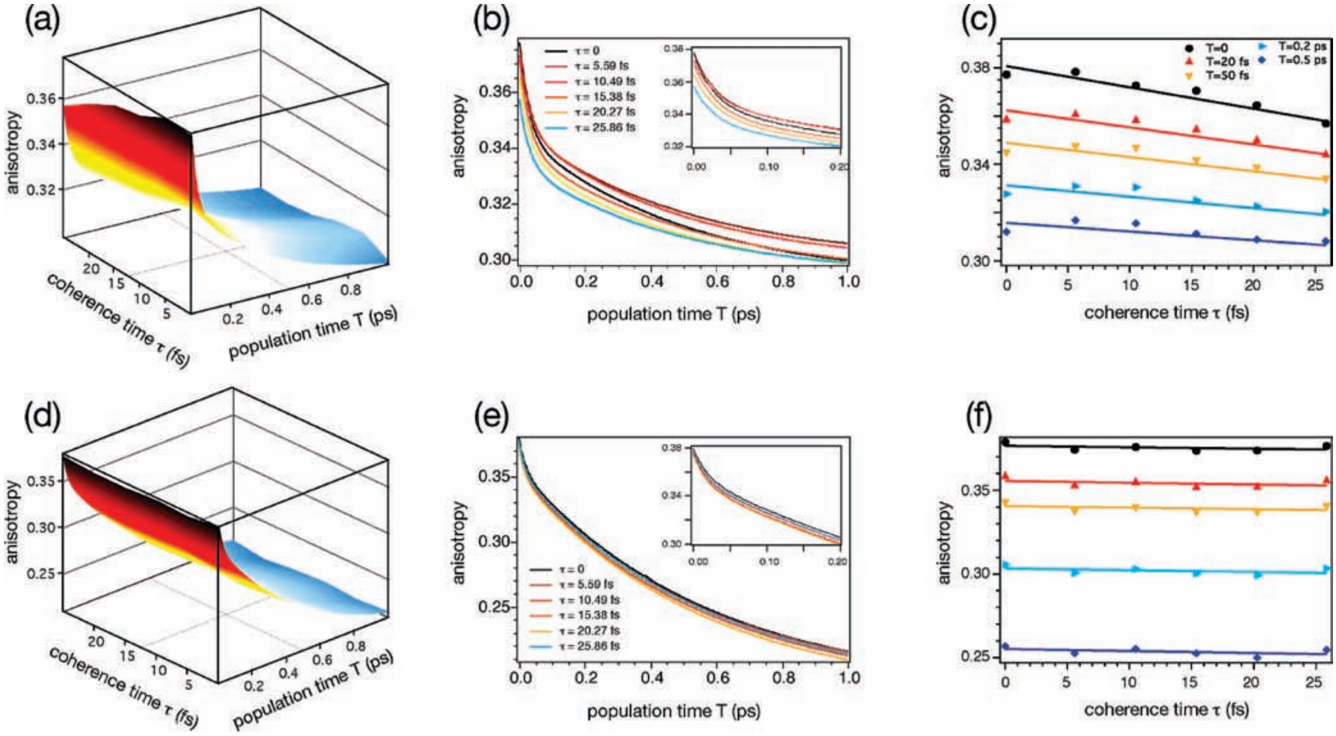

Figure 6. TTAD experimental results obtained for CF solution (a−c) and NP suspension (d−f). (a) and (d) 3D plots showing the anisotropy decays as function of both T and τ. (b) and (e) Slices through the experimental surface along T at selected values of τ (fitted curves are reported for clarity). (c) and (f) Slices through the experimental surface along τ at selected values of T: dots represent the experimental points whereas the solid lines represent linear fits as guide for the eye. All the reported data are the average of at least 9 repeated measurements.

parameters are reported in the Supporting Information accompanying ref 42. As in conventional anisotropy experiments, these traces provide information about transition dipole moment reorientation during the excited-state lifetime. In the case of these experiments, decay of anisotropy is caused primarily by EET. It is evident that the anisotropy decays over the first picosecond of T more significantly for NPs compared to MEH-PPV in the chloroform solution. The behavior of the anisotropy as a function of T can be interpreted similarly to numerous reports focused on the study of the depolarization dynamics in a wide range of polymers and their aggregation states.[51,57,117,183−188] Those studies suggest that the photophysics of polymeric chains, in particular their depolarization dynamics, are strongly dictated by the conformation they assume. In samples characterized by a more closely packed morphology, like thin films, NP suspensions, or solutions in poor solvents where polymers assume highly folded conformations, interchain interactions are maximized, enabling efficient three-dimensional EET. This efficient interchain EET is observed as faster depolarization dynamics in the anisotropy decay traces and as a large Stokes shift in the fluorescence spectrum.

We observe that the initial ($T = \tau = 0$) anisotropy is lower than the theoretical value of 0.4 expected for two-level systems, being 0.38 ± 0.05. Similar observations have been previously reported for thin films of polythiophene[184] as well as concentrated[57] and diluted[61] solutions of phenylenevinylene derivatives. The low initial anisotropy has been attributed to an ultrafast process decaying the anisotropy within the finite pulse duration. Ultrafast relaxation processes (~25 fs) were also found by 3PEPS.[93,163,171] Recent studies based on correlated semiempirical quantum-chemical calculations[61] and a theory for exciton relaxation,[89,90,189] have postulated that this ultrafast component can be ascribed to a relaxation process through a manifold of exciton population states, associated with rapid localization of the excitation because of the dominance of conformational disorder.

Panels c and f show the decay of anisotropy along τ. The figure immediately highlights a dependence of the anisotropy signal along the τ axis for the CF solution but not for the NP suspension. Owing to the experimental design, this result shows that coherence EET occurs after excitation of extended conformation MEH-PPV chains, but not in collapsed-chain NPs. Moreover, it is remarkable that this phenomenon occurs at room temperature. We would expect, indeed, that at room temperature the dephasing time is fast enough to destroy any coherence information within tens of femtoseconds.[33]

These data lead to two conclusions that seem to go against the common assumptions about the EET process. First, quantum coherence effects were experimentally recorded at room temperature, when the decoherence time, meaning the time during what the system can retain memory of the initial phase information, is estimated to be at most ~10 fs (based on the photon echo signal).[33] Second, this quantum effect was recorded in CF solutions but not in NP suspensions, even though the close-packing morphology in NPs should guarantee a stronger coupling U and, in turn, a better probability to observe coherence transfer.

An explanation of both these controversial points can be found by resorting to the concept of cross-correlation functions. In other words, we conclude that it is the dephasing mechanism rather than time scale that is of paramount importance. The TTAD experiment can detect coherent excitation transport only if the cross correlation functions ξ_{ad} do not vanish. In other words, a decay of anisotropy along τ can be recorded only if the transition frequencies of the donor and the acceptor are correlated. This can happen, for example, in the strong coupling limit during the relaxation from an upper to a lower delocalized exciton state. When donor and acceptor are strongly coupled, their electronic states mix to produce a new delocalized excitonic state. Relaxation through this manifold of exciton states retains the averaged correlation between the transition frequencies of single chromophores because of the delocalized nature of such states. The formation of these excitonic states is known in the case of aggregate chains, like in films or NPs.[15] However, since no decay along τ was recorded for NP samples, this kind of relaxation is likely to be dominated by evolution of populations, not coherences, consistent with our recent modeling.[61] This kind of relaxation process was invoked to explain the ultrafast decay component recorded in 3PEPS experiments[93,163,171] as well as in depolarization measurements.[57,117,188] Our TTAD results, in particular the ones for NPs, suggest that this relaxation mechanism has to be considered to explain the overall ultrafast dynamics of the EET process—in particular to justify the initial value of anisotropy—but it does not lead to the decay of anisotropy along τ.

Having ruled out the exciton relaxation mechanism, an explanation for the τ-decay of the anisotropy can be suggested by considering the different energy migration pathways in the two analyzed samples. Interchain EET is expected to be the main process in NPs where the close-packing morphology promotes chain−chain contacts. On the other hand, the relatively open-chain configuration assumed by the polymer in CF promotes energy migration between adjacent chromophores (intrachain EET). In a previous contribution we suggested that the anisotropy decay along τ recorded in CF solutions can be explained by thinking about the σ-bonds connecting the chromophores involved in the excitation migration. The presence of such a strong link helps in “protecting” the correlation between donor and acceptor transition energies at room temperature and guarantees the condition $\xi_{ad} \neq 0$ necessary to observe any coherence effect in the experiment.[42] This assessment will be developed in more detail in section 5 in light of the 2DPE results, from which more information about the actual coherence transfer mechanism can be extracted.

4.3. Model and Simulations. In section 2.3 we showed the conventional definition of anisotropy also holds during the pulse overlap and as a function of either τ and T. We further pointed out that attention has to be paid to pulse ordering and finite pulse duration effects on the relevant Feynman diagrams contributing to the signal. In this section an explicit expression for the anisotropy as a function of the transition dipole moments is derived starting from the definition of the third-order nonlinear response given in eq 15. The aim is to develop a model capable of qualitatively explaining the τ dependence found in the TTAD results. The first step is the explanation of the orientational averages formalism, necessary to account for the photoselection exerted by the polarized pump pulses and the subsequent polarized probe step. The Feynman diagrams illustrating the relevant Liouville space pathways contributing to the TTAD signal will be then identified and the total nonlinear response function will be calculated by summing over these contributions, as shown in eq 17.

In general, an observable describing light−matter interaction at the $(n - 1)$th order of a nonlinear optical spectroscopy can be expressed as[59,122,124,125]

$$C^{(n)} = \langle S_{i_1,...,i_n} T_{i_1,...,i_n} \rangle \tag{19}$$

where $\langle ... \rangle$ denotes the orientational average, $S_{i_1,...,i_n}$, is the field polarization tensor and $T_{i_1,...,i_n}$ is the molecular response tensor, both defined in a fixed (laboratory) frame chosen so that the elements of $S_{i_1,...,i_n}$ can be easily expressed. It is this function, describing how the experimenter can photoselect electronic transitions in an ensemble and then probe their reorientation (e.g., caused by EET) that dictates the decay of an anisotropy experiment. The main difference between TTAD and typical experiments like fluorescence anisotropy is that TTAD is a third-order coherent spectroscopy so that eq 19 is a rank 4 average with two time delays.

For a randomly oriented system $T_{i_1,...,i_n}$ can be conveniently expressed in a local molecular frame as

$$T_{i_1,...,i_n} = l_{i_1\lambda_1} \dots l_{i_n\lambda_n} T_{\lambda_1,...,\lambda_n} \tag{20}$$

where $l_{i_j\lambda_j}$ are the direction cosines of the angles between the fixed (i_j) and molecular (λ_j) axes. For a multilevel system $T_{\lambda_1,...,\lambda_n}$ can be expressed as a product of n electronic transition dipole moments, whose sequence is determined through a diagrammatic expansion of the induced polarization.

To calculate the rotational average of the observable $C^{(n)}$ it is necessary to calculate the rotational average of the direction cosines product $l_{i_1\lambda_1} ... l_{i_n\lambda_n}$. Following Andrews and Thirunamachandran,[125] the rotational average of this product for third-order spectroscopies ($n = 4$) can be expressed in Cartesian tensor form as[59]

$$I_{abcd;\alpha\beta\gamma\delta} = \frac{1}{30}\begin{bmatrix}\delta_{ab}\delta_{cd}\\ \delta_{ac}\delta_{bd}\\ \delta_{ad}\delta_{bc}\end{bmatrix}^T \begin{bmatrix}4 & -1 & -1\\ -1 & 4 & -1\\ -1 & -1 & 4\end{bmatrix} \begin{bmatrix}\delta_{\alpha\beta}\delta_{\gamma\delta}\\ \delta_{\alpha\gamma}\delta_{\beta\delta}\\ \delta_{\alpha\delta}\delta_{\beta\gamma}\end{bmatrix} \tag{21}$$

where δ_{il} are Kronecker deltas with $a-d$ and $\alpha-\delta$ subscripts labeling the electric fields in the fixed frame (E_1, E_2, E_3, E_S, respectively), and the corresponding response in the molecular frame (the transition dipole moment vectors).

Combining eq 21 with eqs 19 and 20, and considering a signal polarization radiated in the $-\mathbf{k}_1 + \mathbf{k}_2 + \mathbf{k}_3$ direction, it is found that

$$C^{(4)} = \frac{1}{30}\begin{bmatrix}(\hat{e}_a^*\hat{e}_b)(\hat{e}_c\hat{e}_d^*)\\ (\hat{e}_a^*\hat{e}_c)(\hat{e}_b\hat{e}_d^*)\\ (\hat{e}_a^*\hat{e}_d^*)(\hat{e}_b\hat{e}_c)\end{bmatrix}^T \begin{bmatrix}4 & -1 & -1\\ -1 & 4 & -1\\ -1 & -1 & 4\end{bmatrix} \begin{bmatrix}(\hat{\mu}_\alpha^*\hat{\mu}_\beta)(\hat{\mu}_\gamma\hat{\mu}_\delta^*)\\ (\hat{\mu}_\alpha^*\hat{\mu}_\gamma)(\hat{\mu}_\beta\hat{\mu}_\delta^*)\\ (\hat{\mu}_\alpha^*\hat{\mu}_\delta^*)(\hat{\mu}_\beta\hat{\mu}_\gamma)\end{bmatrix} \tag{22}$$

where $\hat{e}_i$ and $\hat{\mu}_\lambda$ are the field polarizations and transition dipole moment vectors, respectively, and asterisk indicates the complex conjugate. The field polarization tensor (first term in eq 22) can be easily calculated as $[1\ 1\ 1]^T$ for the parallel component and $[1\ 0\ 0]^T$ for the perpendicular one. The explicit form of the molecular response tensor $\mathbf{T}$ can then be determined starting from the appropriate double-sided Feynman diagrams (Figure 7).

Diagram a in Figure 7 represents the conventional anisotropy experiment. The time delay τ between the two pump pulses is fixed to zero and population transfer (EET) is considered during T. Starting from the expression of $\mathbf{T}$ associated with this diagram and combining eq 13 with eqs 19−22, we obtain the conventional expression of anisotropy in terms of the mean angle between transition dipoles

$$r(T) = \frac{1}{5}(3\cos^2\phi(T) - 1) \tag{23}$$

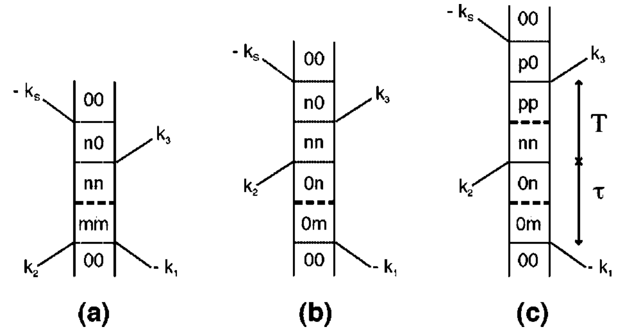

Figure 7. Double-sided Feynman diagrams for the nonlinear third-order polarization in the $-\mathbf{k}_1 + \mathbf{k}_2 + \mathbf{k}_3$ phase matching direction in the impulsive limit accounting for coherence dynamics as measured by the two-time anisotropy decay experiment. The bold dashed lines denote population or coherence transfer occurring during T and τ, respectively.

with the angle ϕ defined as the time-dependent ensemble average angle between $\hat{\mu}_m$ and $\hat{\mu}_n$. The same procedure can be followed to derive an analogous expression for the TTAD experiment. The easiest way to include coherence transfer processes in this description is shown in diagram b. However, the expression of anisotropy derived from eqs 13 and 19−22 obtained for that diagram does not show any dependence on the angle between the transition dipole moments nor, consequently, on the coherence time. While that is a mathematical finding, a plausible physical interpretation is that the anisotropy decays only when there is a change in dipole orientation in two coherence periods.

It was therefore found that a necessary condition to obtain a dependence of anisotropy on τ is to assume a second EET event during the population time, as shown in diagram c. In this case the anisotropy decay as functions of τ and T is calculated to be

$$r(\tau,T) = \frac{1}{5}\left(\frac{3\cos\psi(\tau,T)\cos\phi(T)}{\cos\theta(\tau)} - 1\right) \tag{24}$$

where θ [$=\theta(\tau)$], ϕ [$=\phi(T)$], and ψ [$=\psi(\tau,T)$] are the angles between the ensemble averaged transition dipole moment vectors at different points in time, ($\hat{\mu}_m$, $\hat{\mu}_n$), ($\hat{\mu}_n$, $\hat{\mu}_p$), and ($\hat{\mu}_m$, $\hat{\mu}_p$), respectively, according to the Feynman diagrams in Figure 7c. In this model the coherence transfer must be followed by a population transfer in order for the anisotropy to show any dependence on the τ delay.

The anisotropy decays as a function of τ and T were simulated using eq 24, assuming that the major contribution to the signal in the TTAD experiment is carried by diagram c in Figure 7. The signal from a conventional experiment (diagram a) was also studied for comparison. The temporal dependence of the ensemble average angles $\theta(\tau)$ and $\phi(T)$ were modeled with Boxlucas functions (i.e., having the form $1 - \exp(-kt)$), assuming that at infinite time they assume the magic angle value (54.7°) corresponding to a complete depolarization of the signal. Their time constants are indicated as $1/k_\tau$ and $1/k_T$, respectively. It was assumed that the two-time angle function $\psi(\tau,T)$ can be described approximately in terms of sequential kinetics where $\phi(T)$ rotation follows $\theta(\tau)$ rotation. The simulation results are compared with the experimental ones in Figure 8.

Owing to the fact that coherence EET can only be measured when it is followed by population EET, its presence is hidden in TTAD unless the time scales for the two processes are similar. We found that when the dynamics along τ are set significantly slower or faster than the dynamics along T, no noticeable dependence of anisotropy decay from τ is recorded. This mimics the experimental results for the NP suspension (not shown). On the other hand, when the two time scales are similar, a clear dependence along the τ axis is found and the same highly nonexponential behavior of anisotropy at early time, like the experimental data for the CF solution, can be reproduced, Figure 8c. Owing to the rapid dephasing, in particular since the measurements were performed at 293K, it was not possible to establish the functional form of the τ-dependence. That is because the absolute signal intensities decay strongly with τ, which degrades the signal-to-noise ratio of the anisotropy.

Finite pulse duration was taken into account carefully since it may introduce nontrivial effects into the third-order nonlinear signals, especially if the time scales of the investigated processes are comparable to the pulse duration. In our simulations the temporal field envelope was assumed to be Gaussian—as suggested by the experimentally measured time−bandwidth product—and its width (fwhm 30 fs) was determined on the basis of autocorrelation experiments.

The pulse duration has a substantial influence on the simulation results through its effect on the initial value of the anisotropy: as the pulse duration is increased, the initial value of anisotropy ($\tau = T = 0$) progressively decreases from the theoretical value of 0.4. Although this is true for both the conventional anisotropy as well as the TTAD experiment, the effect is more significant in the latter. As mentioned in the former sections, previous work justified the lower value of initial anisotropy by invoking fast EET as a function of T together with consideration of finite pulse durations. However, the results of our simulation show that the initial value of anisotropy is also affected by coherence transfer, according to the relative magnitude of the time constants k_τ and k_T. In the present work, careful choice of these constants enabled us to reproduce the initial values of anisotropy at different τ for both the samples studied, Figure 8d.

Another important point emerging from the simulations is that, even if the initial value of anisotropy is dependent on pulse duration, its functional form along τ and T depends critically only on the peak-to-peak time delay between pulses (i.e., τ and T). Through these simulations we find that, even if the range of τ investigated is comparable to pulse duration, the experiment allows us to detect coherent dynamics—those that depend explicitly on τ—with time scales comparable to or faster than the pulse duration. This is intrinsically connected with the nonlinear power dependence of nonlinear optical signals. A key point to note is that we observe a convincing trend in the data as a function of τ (and T).

4.4. Quantum Beats in Anisotropy. An anisotropy trace along T for the MEH-PPV/CF sample, together with a multi-exponential fit and a plot of the residuals of this fit, are shown in Figure 9. The residuals show clear oscillations lasting over a picosecond. The Fourier analysis of the beats reveals two main frequencies, at 255 and 366 cm^{-1}. Similar oscillations in the anisotropy decay as a function of T were detected at all the different values of τ investigated. No variations in the amplitude, phase, or frequency of these oscillations were detected as function of τ within the experimental noise. We detected similar oscillations, though with smaller amplitude, in the aqueous NP suspensions and in dilute MEH-PPV/toluene solutions (data not shown). It therefore seems to be unlikely that these oscillations are CF solvent Raman modes at 261 and 366 cm^{-1}. A Raman mode with a frequency of 327 cm^{-1} has been reported for PPV chains.[190−194]

Oscillations are commonly observed in ultrafast optical spectroscopies. In particular, it is well-known that the oscillations

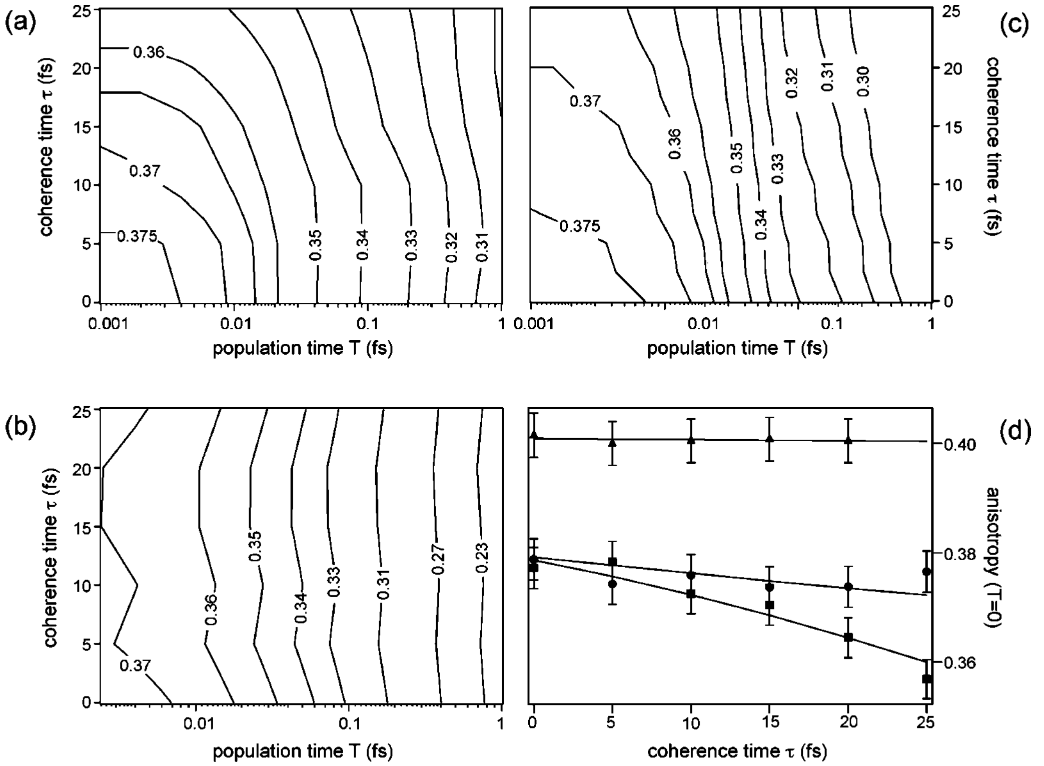

Figure 8. Experimental TTAD surfaces as a function of τ and T for (a) MEH-PPV in chloroform solution and (b) MEH-PPV NP suspension in water. (c) Simulation results using a multiexponential model and realistic pulse duration to mimic the experimental data for the chloroform solution; $k_{T1} = 0.05$, $k_{T2} = 0.002$, and a static offset, $k_{\tau 1} = 1.0$, $k_{\tau 2} = 0.2$, $k_{\tau 3} = 0.1$ fs^{-1}. This simulation shows that the experiment can resolve ultrafast dynamics occurring on the time scale of the pulse duration (~30 fs). (d) Anisotropy values calculated at $T = 0$ as function of coherence time for rhodamine 6G (triangles), MEH-PPV solution in chloroform (squares) and aqueous MEH-PPV NP suspension (circles). The points are averages, and the error bars were estimated as standard deviations of repeated measurements. The solid lines are linear fits to the experimental points for rhodamine 6G, whereas they represent slices at $T = 0$ of simulations for the MEH-PPV data.

typically found in ultrafast transient grating, photon echo, pump−probe, etc., data are manifestations of vibrational wavepacket motion that modulates the signal intensity. When the width of the laser pulse is sufficiently shorter than half the period of a molecular vibration, nuclear motion can be coherently induced and vibrational coherences appear as quantum beats, which constitute a simple and well-known example of quantum mechanical interference.[107,113,195,196] The frequency of the resulting oscillation corresponds to the energy separation between the coherently excited vibrational levels. The study and the control of these oscillations have largely been exploited to gain insight into solute−solvent dynamics.[197−201]

It is well-known that the time delay between the first two pulses in four wave mixing experiments can be used to enhance or suppress vibrational coherences by timing the two pulses such that the delay is set in or out of phase with the vibrational mode. This method is known as coherence control or mode suppression.[197−200] In principle, the data as a function of both T and τ could test whether the beats observed in our data can be assigned to normal vibrational wavepackets on the donor chromophore. The range over which we are able to scan τ before the signal is too weak to measure with good signal-to-noise ratio, however, is not wide enough to explore the completely out-of-phase conditions. We estimate that for a mode at 260 cm^{-1}, a 25 fs delay should give a ~20% variation in the relative amplitude of the oscillations. We found no change in the amplitude at various τ, but the results are inconclusive.

Oscillations have been previously observed in anisotropy data. For example, various photosynthetic antenna complexes exhibit oscillations with frequencies on the order of hundreds of cm^{-1}.[44,46,113,202] Oscillations present in each of the vertically

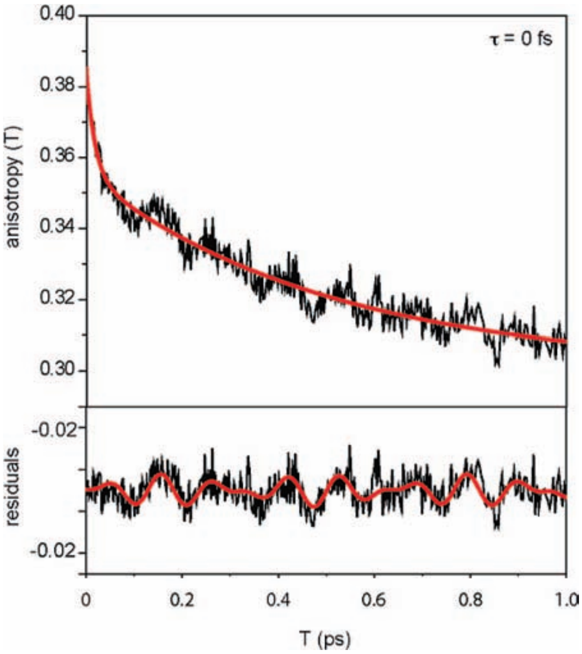

Figure 9. Analysis of residuals from the fit of an example of an anisotropy decay recorded for MEH-PPV/CF solution. (a) Decay of anisotropy along T recorded at $\tau = 0$: black line, experimental points; red line, biexponential plus static offset fit as reported in as reported in ref 42. Oscillations with about the same amplitude, phase, and frequency were recorded also for different values of τ. (b) Oscillatory behavior of the anisotropy: black line, residuals calculated from experimental points; red line, fit with two cosine functions with frequencies 255 and 366 cm^{-1}.

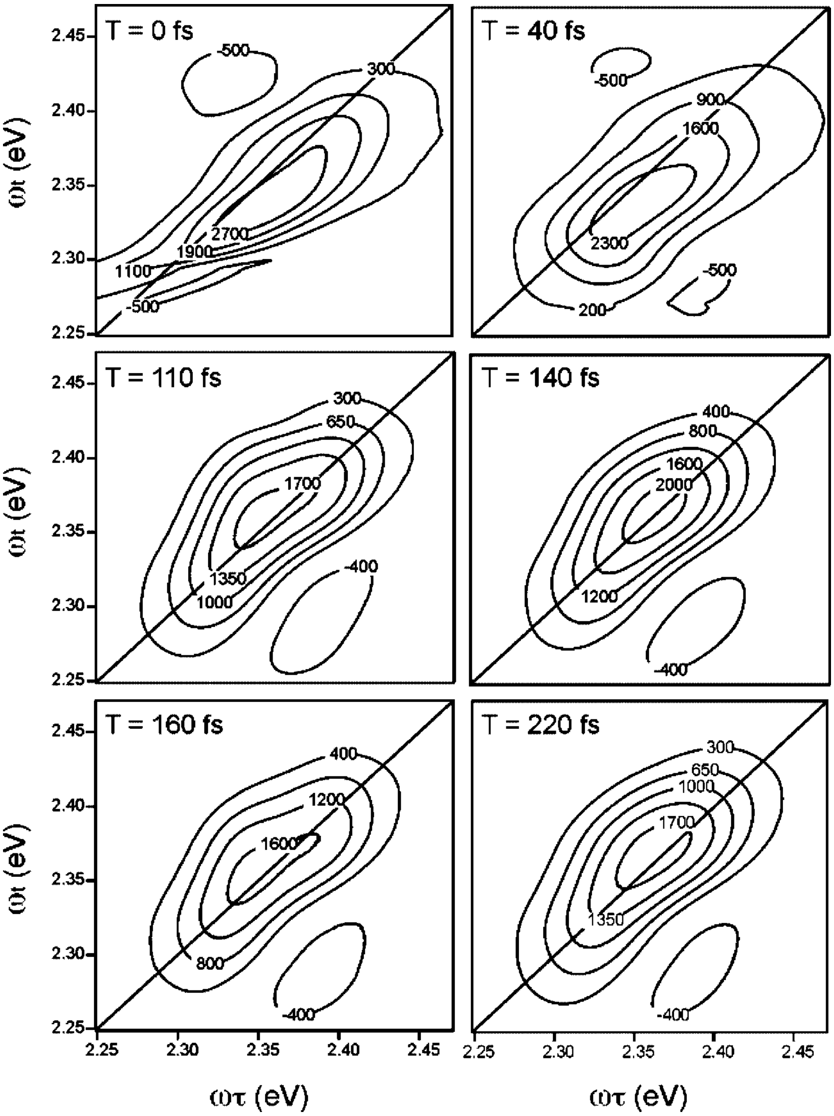

Figure 10. Selected 2D electronic spectra (real part) of MEH-PPV in chloroform solution at $T = 0$, 40, 110, 140, 160, and 220 fs demonstrating the oscillations in the amplitude and in the shape of the diagonal peak.

polarized pump−probe and cross-polarized pump−probe traces normally cancel when anisotropy is calculated. Possible origins of anisotropy beats have been discussed previously in the literature.[44,46,202,203] Recall that anisotropy is sensitive to any process involving a change in the transition dipole orientation, say from $\vec{\mu}_{0d}$ to $\vec{\mu}_{0a}$, where these transition dipole moments generally differ in direction. When excitation energy is transferred from the donor to the acceptor under conditions of weak coupling, the anisotropy decay follows an exponential law because the EET rate constant dictates the decay of the dipole projection correlation function. On the other hand, in the intermediate−strong coupling regime, electronic oscillations can occur in the acceptor state population as a function of time. Consequently, the dipole projection correlation function oscillates with the same frequency, causing beats in the anisotropy decay.

The long damping time of the oscillations in our data (~1 ps) suggests that it is unlikely that they can be assigned to a purely electronic coherence. Recent work has examined the entanglement of vibrational and electronic oscillations in the anisotropy decay signals, both in the weak and in the strong coupling regime.[204−206] A detailed study of coupled electronic−nuclear coherence in a molecular dimer system has been reported by Kilin et al.[207] Cina and Fleming show that vibrational coherence transfer from donor to acceptor in a similar model system leads to beats in the anisotropy decay.[204] Furthermore, when the electronic coupling U is sufficiently large compared to γ, the adiabatic potential of excited states becomes distorted. It is then predicted that oscillations can be observed in pump−probe anisotropy, whose frequencies are a combination of U and the vibrational frequencies of the isolated chromophores.[204] Results from the 2DPE technique help to clarify the origins of the MEH-PPV/CF oscillations.

4.5. 2D Photon Echo Results. In Figure 10, representative 2DPE spectra at selected T for MEH-PPV solutions in chloroform are shown. As already discussed in section 2.3, the signal displayed in a 2DPE spectrum is a map correlating the initial frequency ω_τ with the frequency ω_t after a waiting time T. The frequencies ω_τ and ω_t are oscillation frequencies of the system during the conjugate coherence times τ and t. The principal feature in the 2DPE spectra measured for MEH-PPV/CF is a positive, diagonally elongated peak. The diagonal shape means that the radiated signal frequencies (ω_t) are correlated with the initial transition dipole oscillation frequency (ω_τ), signaling inhomogeneous broadening. The extent of the diagonal feature reflects the distribution of the excitation energies produced by absorption of the laser pulse spectrum. We assign the inhomogeneous broadening to the distribution of excitation energies of conformational subunits. The antidiagonal width of the peak indicates the homogeneous broadening.[128]

At early population times ($T < 50$ fs), the main diagonal feature is slightly shifted below the true diagonal as a result of the interplay between the positive (GSB and SE) diagonal signal and negative (ESA, excited-state absorption) contributions on the higher energy side of the diagonal. We attribute the negative peak at ($\omega_\tau = 2.33$ eV; $\omega_t = 2.42$ eV) to ESA to a two-exciton state. This assignment is supported by related experimental and theoretical work showing that, in transient absorption spectra of systems of coupled chromophores pumped close to resonance, ESA occurs to the blue side of the bleaching.[31,208−212] The comparison between the two kinds of experiment is straightforward considering that each vertical slice through a 2D spectrum at a fixed ω_τ, can be associated with a 1D transient absorption trace after excitation at ω_τ.

No significant cross-peaks are observed in the $T = 0$ correlation spectrum, meaning that excitonic coupling between different subunits and correlation among exciton states is initially absent or too small to produce a detectable cross-peak. Starting from $T > 40$ fs, a negative cross feature on the lower energy side of the diagonal ($\omega_\tau = 2.38$ eV; $\omega_t = 2.29$ eV) appears. The feature grows in intensity over the first 100 fs after photoexcitation and persists for longer than 1 ps. The fact that the peak appears below the diagonal means that the state initially excited had a higher energy than the final state. One possible explanation of the feature is ESA from a conformational subunit that absorbs to the red of the laser spectrum and that has been rapidly sensitized by EET.

EET dynamics in this class of polymers predominantly occur on time scales that are on the order of picoseconds, mainly consistent with hopping (weak coupling) models.[51,57,61,118,183,185−187] The red-shifted ESA feature in the 2DPE data is populated much more rapidly and might form via similar relaxation/localization processes proposed to explain the ultrafast decay in 3PEPS[163,171] and depolarization experiments.[57,61,117] Ultrafast relaxation of a state absorbing in the vicinity of the MEH-PPV/CF absorption maximum could thereby relax to a red-shifted excited state mainly localized on a longer/straighter subunit of the chain, not initially populated by the excitation pulse. However, we note that, even though excitons are considered to be the dominant species formed immediately upon ultrafast excitation of MEH-PPV in dilute solution, a possible contribution to the dynamics from other photogenerated species cannot be completely discounted. The role of polaron pairs and excimers in deciding the early time polymer photophysics has been recently discussed in the literature.[213−215] We cannot rule out the possibility that the red-shifted ESA feature is due to polaron pair formation.

Polaron pairs are species where the electron and the hole are on different conformational subunits but are still bound.[182,216] Although the mechanism of free charge formation remains polemical, there is a general consensus that these species are formed fast (<100 fs) though in small yield (<3%).[162,214,215,217] Recently, evidence of excimer formation was also detected in MEH-PPV films,[218] but it was found to be negligible in solutions. Signatures of polaron states in the 2DPE response would be particularly interesting since it would represent proof for the photogeneration of polaron pairs at early times, and it would contribute to understanding the still largely unknown problem of the nature of the primary photogenerated species. On the fastest time scales, intrachain formation of a coherently coupled exciton−polaron resonance is equivalent to exciton delocalization caused by orbital overlap-dependent interactions.[219,220] It is therefore possible that polaron pairs could be involved in deciding the interplay of excitation localization/delocalization dynamics. The ultrafast formation of polaron pairs signaled by the red ESA feature in the 2DPE data is an interesting idea that cannot be discounted. However, in the present work we focus on the EET dynamics.

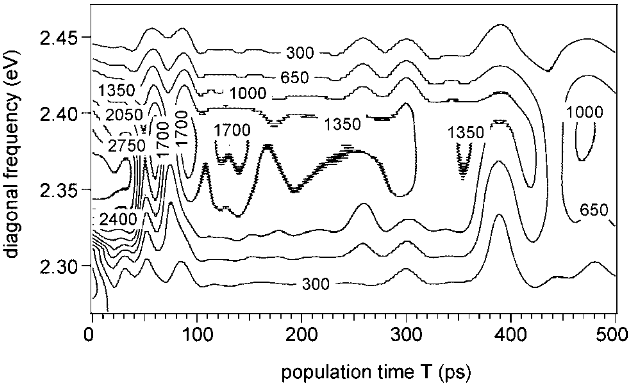

Figure 11. Contour plots of the amplitude of the spectra along the diagonal line as a function of frequency and population time.

Analyzing in more detail the dynamics of the main peaks during T, we note that the decay of the diagonal peak is not monotonic. The comparison between 2DPE spectra measured at different T reveals the presence of an oscillation in the amplitude and in the shape of this peak, which becomes rounder as it gets stronger. The presence of this oscillation is more evident after extracting the amplitudes of the spectra along the diagonal line and plotting it as a function of frequency and T, Figure 11.

Fourier transform analyses were carried out on three series of independent experiments to extract the frequencies of the oscillations. Different horizontal slices through the 2D surfaces, evident in Figure 10, were furthermore taken into account, but no frequency or amplitude dependence on the wavelength was detected within the experimental error. Traces within the same experimental series were then analyzed with a single-value-deconvolution method, allowing estimation of the frequencies and amplitudes of the oscillations. The final results, obtained as the average of the three different series of experiments, highlight the presence of two main frequency components (230, 350 cm^{-1}) together with weaker higher frequency components (445, 575 cm^{-1}). The error associated with these measured frequencies is estimated to be about ±30 cm^{-1}. Interestingly, the two lowest frequency components correspond, within the experimental uncertainty, to those found in anisotropy decays, suggesting a common origin for these beats.

The same analysis carried out along the antidiagonal direction showed similar oscillations, with similar frequencies within the experimental error. Although the presence of such antidiagonal oscillations was confirmed in all sets of recorded data, it was not possible find a reproducible phase relationship between diagonal and antidiagonal beats.

An important concept, described mainly in work from the Fleming group, is that 2DPE spectroscopy can be used to ascertain whether oscillations are caused by nuclear or electronic coherences.[40,41] The 2DPE data can therefore help to resolve more clearly the origin of the oscillations we observe in the anisotropy decays, because we see similar oscillations in the diagonal intensity in the 2DPE data. We find that the oscillations in the MEH-PPV/CF data influence both the amplitude and the shape of the main peak in the 2DPE data, where the shape of

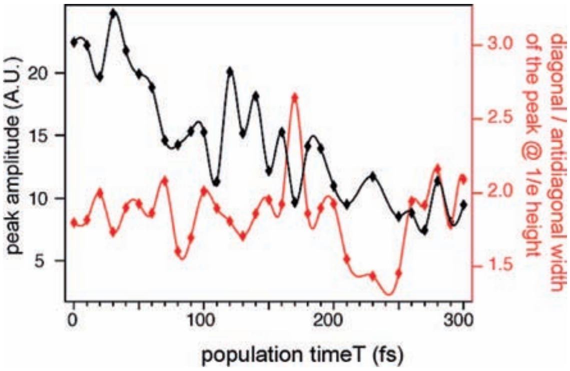

Figure 12. Comparison between the amplitude of the diagonal peak (left axis, black line) and the ratio between the diagonal and antidiagonal widths of the peak at 1/*e* height (right axis, red line). These data are an average of three independent experiments. The lines show the characteristic anticorrelation theoretically predicted for oscillations caused by electronic coherences.

a peak is defined as the ratio of diagonal to antidiagonal widths at 1/*e* height.[40,133,137] In Figure 12 we compare the peak amplitude and shape oscillations at 2.38 eV, corresponding to the maximum signal (Figure 11), resulting from an average of three independent experiments. According to previous experimental[133,221] and theoretical studies,[103,133,137] the clear anticorrelation we observe between the two plots represents strong evidence that electronic coherences are involved here, rather than purely vibrational coherences. The frequencies of the oscillations are primarily indicative of intramolecular vibrational motions (of MEH-PPV); therefore we conclude that the oscillations in the anisotropy and 2DPE data, as a function of T, are mixed vibrational−electronic coherences. Our evidence is somewhat indirect because we do not see clearly resolved cross-peaks in the 2DPE data.[222] Nonetheless, the anticorrelation in the intensity and shape of the 2DPE data suggests that electronic coherences contribute (intermediate coupling) for the first ∼250 fs after photoexcitation. The anisotropy data suggest that vibrational coherence among donor and acceptor persists for ∼1 ps. These findings complement and support the results obtained with the TTAD technique, strengthening our conclusion that quantum transport effects can occur at ambient temperature along conjugated polymer chains.[42]

5. Concluding Remarks

We have reported the results of ulfrafast spectroscopic investigations of EET in the prototypical conjugated polymer MEH-PPV. We focused on the possible role that coherent effects can have in EET dynamics for systems described by the intermediate coupling regime. Two different structural forms of MEH-PPV were used as model multichromophoric systems. Together with the 2DPE technique, already demonstrated to be sensitive to coherence transfer along the population time T, a new technique (TTAD) based on the anisotropy decay detection as function of two times, T and τ, was specifically designed and applied to measure coherent EET. A simple model based on the response−function formalism was developed to validate the results obtained with the TTAD technique. It was demonstrated that TTAD directly detects coherent EET occurring during τ, because transfer of electronic coherences from one chromophore to another can decay the anisotropy along τ. The TTAD τ-dependent anisotropy data suggest that this kind of coherence transfer—through space—does occur, predominantly in the case of intrachain transport. That result means that the dynamics of intrachain EET in MEH-PPV cannot be properly captured by theoretical models that employ the secular approximation. That is, populations and coherences evolve in concert on ultrafast time scales.

Although the TTAD technique directly records evidence for coherent EET during τ, it cannot distinguish the underlying mechanism. On the other hand, the 2DPE technique detects the effect of coherent superpositions of excitons on the population dynamics as beats in the peak amplitude and by changes along the diagonal and antidiagonal shape. It can provide more information about the mechanism and the nature of vibrational coherences also involved in EET. As described in section 4.5, the main peak amplitude shows oscillations along both the diagonal and the antidiagonal directions. The results obtained with the 2DPE experiment established that long-lived electronic coherences exist for at least 250 fs after photoexcitation of MEH-PPV in chloroform solution at 293 K. These electronic coherences involve superpositions of donor and acceptor states, and they are intimately mixed with vibrational coherence transfer that lasts for ∼1 ps. Both these observations suggest the need for a nonequilibrium theory that considers common bath modes. Our results, indeed, provide a rich demonstration of concepts such as those described by Jang, et al.[30] We hope our observations motivate further development and application of such theories.

Fleming and co-workers have also reported long lasting electronic coherences recorded using the 2DPE method for a light-harvesting antenna protein called the FMO complex.[41,133] They suggested that the common protein bath in which the different chromophores are embedded helps to preserve the correlation between energy gaps over time scales substantially longer than the decoherence time estimated from the correlation function of the transition frequency.[221] In other words, coherences can be maintained for a much longer duration than the period we normally consider to be the decoherence time for the system if some bath fluctuations are correlated among the donor and acceptor sites. Recent 2C-3PEPS (two-color, three-pulse photon echo spectroscopy) measurements on polythiophene have been reported by Wells and Blank.[160] They suggest that vibrational torsional modes could play an important role in retaining spectral correlation during relaxation, which may be related to our observations for MEH-PPV.

There has been recent interest in how EET dynamics can occur without being as limited by the system decoherence time as previously thought.[223,224] Some researchers are suggesting that the answer might only be discovered using fairly detailed models for the bath.[41,72,225] Some time ago Laird and Skinner showed that the T_2 dephasing time can actually be longer than the population relation time (T_1) in a two-level quantum system linearly coupled to a thermal bath modeled using a finite temperature model.[226] Recently, Dunkel et al. have explored a similar model system and also found cases where dephasing was slower than population relaxation.[227] They make the interesting suggestion that decoherence times can be lengthened when the bath is prepared in a nonequilibrium state. A possible example of this is when the system drives the bath out of equilibrium, perhaps by intramolecular vibrational motions.

Correlation between the fluctuations of the donor and acceptor transition frequencies, $\xi_{ad} \neq 0$, is necessary to detect coherent EET in the TTAD experiment. Therefore, there must be some correlation in the bath along MEH-PPV chains in solution. A likely source of the correlated fluctuations is the chemical bonds connecting the donor and the acceptor chromophores. This makes a lot of sense if we consider vibrational modes that span more than one conformational subunit. The long-lived vibrational coherences noted in the anisotropy and 2DPE data further strengthen this idea because a single vibrational mode spanning donor and acceptor helps to explain why the vibrational coherence transfer persists for approximately 1 ps, a time scale more in accord with the decoherence time of vibrational quantum beats on a single chromophore. This, in turn, emphasizes the ways that spectral overlap can be quite interesting in the intermediate coupling regime—evidently Franck−Condon factors for EET evolve in time, much like in resonance Raman spectroscopy,[228,229] because our observations cannot be predicted by models that average over equilibrium Franck−Condon factors for the donor emission and acceptor excitation independently.

The concept of spectral overlap is important in EET theory, and it may furthermore provide a clue as to why electronic coherence can be preserved between conformational subunits along MEH-PPV chains, despite the fact that there is substantial energetic disorder in the site energies. Common vibrations among chromophores with different electronic transition frequencies can be employed to make the donor emission frequency approximately equal to the acceptor absorption frequency, thus enhancing electronic mixing. In this case, the strongest interchromophore coherences must involve coupled electronic and vibrational levels. In a sense, the vibronic ladder can help to offset disorder in the nonequilibrium limit.

Our results show that a number of interesting effects are present in the intermediate coupling regime for EET. This complexity inherent in the system highlights the deficiency of treating the nuclear motions as contributing a single dephasing parameter that ultimately limits whether or not quantum coherent dynamics can occur. We further conclude that the common structural framework of the macromolecule introduces correlation in the energy gap fluctuations that, in turn, preserves the coherence and permits coherent EET, even at room temperature. It will be of great interest in the future to compare different kinds of structures that connect donor and acceptor chromophores.

Acknowledgment. The Natural Sciences and Engineering Research Council of Canada is gratefully acknowledged for support of this research. G.D.S. acknowledges the support of an EWR Steacie Memorial Fellowship. The authors thank J. Kim for his help in the assembly of the experimental setup and A. M. Moran for computer code. We thank V. M. Huxter and C. Y. Wong for their comments on the manuscript.

References and Notes

(1) Scholes, G. D. *Annu. Rev. Phys. Chem.* **2003**, *54*, 57–87.

(2) Holden, D. A.; Guillet, J. E. *Macromolecules* **1980**, *13*, 289–295.

(3) Ghiggino, K. P.; Yeow, E. K. L.; Haines, D. J.; Scholes, G. D.; Smith, T. A. *J. Photochem. Photobiol., A* **1996**, *102*, 81–86.

(4) Adronov, A.; Frechet, J. M. J. *Chem. Commun.* **2000**, 1701–1710.

(5) Varnavski, O.; Samuel, I. D. W.; Palsson, L. O.; Beavington, R.; Burn, P. L.; Goodson, T. *J. Chem. Phys.* **2002**, *116*, 8893–8903.

(6) Goodson, T. *Annu. Rev. Phys. Chem.* **2005**, *56*, 581–603.

(7) McQuade, D. T.; Hegedus, A. H.; Swager, T. M. *J. Am. Chem. Soc.* **2000**, *122*, 12389–12390.

(8) Swager, T. M. *Chem. Rev.* **2007**, *107*, 1339–1386.

(9) Gobets, B.; van Grondelle, R. *Biochim. Biophys. Acta* **2001**, *1507*, 80–99.

(10) van Grondelle, R.; Novoderezhkin, V. I. *Phys. Chem. Chem. Phys.* **2006**, *8*, 793–807.

(11) Scholes, G. D.; Fleming, G. R. *J. Phys. Chem. B* **2000**, *104*, 1854–1868.

(12) Scholes, G. D.; Fleming, G. R. In *Adventures in Chemical Physics: A Special Volume of Advances in Chemical Physics*; Berry, R. S., Jortner, J., Eds.; J. Wiley: Hoboken, NJ, 2006.

(13) van Grondelle, R.; Dekker, J. P.; Gillbro, T.; Sundstrom, V. *Biochim. Biophys. Acta* **1994**, *1187*, 1–65.

(14) Scholes, G. D.; Rumbles, G. *Nat. Mater.* **2006**, *5*, 683–696.

(15) Scholes, G. D.; Rumbles, G. In *Annual Review of nano research*; Cao, G., Brinker, C. J. , Ed.; World Scientific: NJ, 2008; Vol. 2.

(16) Greenham, N. C.; Moratti, S. C.; Bradley, D. D. C.; Friend, R. H.; Holmes, A. B. *Nature* **1993**, *365*, 628–630.

(17) Halls, J. J. M.; Walsh, C. A.; Greenham, N. C.; Marseglia, E. A.; Friend, R. H.; Moratti, S. C.; Holmes, A. B. *Nature* **1995**, *376*, 498–500.

(18) *Semiconducting polymers: Chemistry, physics and engineering*, 2nd ed.; Hadziioannou, G., Malliaras, G. G., Eds.; Wiley-VCH: Weinheim, 2007.

(19) Brédas, J. L.; Chance, R. R. *Conjugated polymeric materials: opportunities in electronics, optoelectronics and molecular electronics*; Kluwer: Boston, 1990.

(20) Kenkre, V. M.; Knox, R. S. *Phys. Rev. B* **1974**, *9*, 5279–5290.

(21) Kakitani, T.; Kimura, A.; Sumi, H. *J. Phys. Chem. B* **1999**, *103*, 3720–3726.

(22) Kimura, A.; Kakitani, T.; Yamato, T. *J. Phys. Chem. B* **2000**, *104*, 9276–9287.

(23) Rackovsky, S.; Silbey, R. *Mol. Phys.* **1973**, *25*, 61–72.

(24) Scholes, G. D.; Ghiggino, K. P. *J. Chem. Phys.* **1994**, *101*, 1251–1261.

(25) Varnavski, O.; Ostrowski, J. C.; Sukhomlinova, L.; Twieg, R. J.; Bazan, G. C.; Goodson, T. *J. Am. Chem. Soc.* **2002**, *124*, 1736–1743.

(26) Simpson, W. T.; Peterson, D. L. *J. Chem. Phys.* **1957**, *26*, 588–593.

(27) Silbey, R.; Harris, R. A. *J. Chem. Phys.* **1984**, *80*, 2615–2617.

(28) Chandler, D.; Wolynes, P. G. *J. Chem. Phys.* **1981**, *74*, 4078–4095.

(29) Shapiro, M.; Brumer, P. *Principles of the quantum control of molecular processes*; Wiley-Interscience: Hoboken, NJ, 2003.

(30) Jang, S.; Jung, Y. J.; Silbey, R. *J. Chem. Phys.* **2002**, *275*, 319–332.

(31) Chachisvilis, M.; Kuhn, O.; Pullerits, T.; Sundstrom, V. *J. Phys. Chem. B* **1997**, *101*, 7275–7283.

(32) Kimura, A.; Kakitani, T. *J. Phys. Chem. A* **2007**, *111*, 12042–12048.

(33) Prezhdo, O. V.; Rossky, P. J. *Phys. Rev. Lett.* **1998**, *81*, 5294–5297.

(34) Hwang, H.; Rossky, P. J. *J. Chem. Phys.* **2004**, *120*, 11380–11385.

(35) Anand, S.; Varnavski, O.; Marsden, J. A.; Haley, M. M.; Schlegel, H. B.; Goodson, T. *J. Phys. Chem. A* **2006**, *110*, 1305–1318.

(36) Varnavski, O.; Yan, X.; Mongin, O.; Blanchard-Desce, M.; Goodson, T. *J. Phys. Chem. C* **2007**, *111*, 149–162.

(37) Ranasinghe, M. I.; Varnavski, O.; Pawlas, J.; Hauck, S. I.; Louie, J.; Hartwig, J. F.; Goodson, T. *J. Am. Chem. Soc.* **2002**, *124*, 6520–6521.

(38) Bjorklund, T. G.; Lim, S.-H.; Bardeen, C. J. *J. Phys. Chem. B* **2001**, *105*, 11970–11977.

(39) Zhu, F.; Galli, C.; Hochstrasser, R. M. *J. Chem. Phys.* **1993**, *98*, 1042–1057.

(40) Pisliakov, A. V.; Mancal, T.; Fleming, G. R. *J. Chem. Phys.* **2006**, *124*, 234505.

(41) Engel, G. S.; Calhoun, T. R.; Read, E. L.; Ahn, T. K.; Mancal, T.; Cheng, Y. C.; Blankenship, R. E.; Fleming, G. R. *Nature* **2007**, *446*, 782–786.

(42) Collini, E.; Scholes, G. D. *Science* **2008**, *323*, 369–373.

(43) Lakowicz, J. R. *Principles of Fluorescence Spectroscopy*; Plenum Press: New York, 1983.

(44) Arnett, D. C.; Kumble, R.; Visschers, R. W.; Moser, C. C.; Dutton, P. L.; Hochstrasser, R. M.; Scherer, N. F. *Laser Tech. Condens.-Phase Biol. Syst.* **1998**, *3273*, 244–255.

(45) Cross, A. J.; Fleming, G. R. *Biophys. J.* **1984**, *46*, 45–56.

(46) Savikhin, S.; Buck, D. R.; Struve, W. S. *Chem. Phys.* **1997**, *223*, 303–312.

(47) Varnavski, O.; Menkir, G.; III, T. G.; Burn, P. L. *Appl. Phys. Lett.* **2000**, *77*, 1120–1122.

(48) Min, C.-K.; Joo, T.; Yoon, M.-C.; Kim, C. M.; Hwang, Y. N.; Kim, D.; Aratani, N.; Yoshida, N.; Osuka, A. *J. Chem. Phys.* **2001**, *114*, 6750–6758.

(49) Yeow, E. K. L.; Ghiggino, K. P.; Reek, J. N. H.; Crossley, M. J.; Bosman, A. W.; Schenning, A.; Meijer, E. W. *J. Phys. Chem. B* **2000**, *104*, 2596–2606.

(50) Berberan-Santos, M. N.; Choppinet, P.; Fedorov, A.; Jullien, L.; Valeur, B. *J. Am. Chem. Soc.* **1999**, *121*, 2526–2533.

(51) Gaab, K. M.; Bardeen, C. J. *J. Phys. Chem. A* **2004**, *108*, 10801.

(52) Gaab, K. M.; Bardeen, C. J. *J. Phys. Chem. B* **2004**, *108*, 4619–4626.

(53) Gaab, K. M.; Bardeen, C. J. *J. Chem. Phys.* **2004**, *121*, 7813–7820.

(54) Knox, R. S.; Gulen, D. *Photochem. Photobiol.* **1993**, *57*, 40–43.

(55) Demidov, A. A.; Andrews, D. L. *Photochem. Photobiol.* **1996**, *63*, 39–52.

(56) Brédas, J. L.; Beljonne, D.; Coropceanu, V.; Cornil, J. *Chem. Rev.* **2004**, *104*, 4971–5003.

(57) Ruseckas, A.; Wood, P.; Samuel, I. D. W.; Webster, G. R.; Mitchell, W. J.; Burn, P. L.; Sundström, V. *Phys. Rev. B* **2005**, *72*, 115214.

(58) Heun, S.; Mahrt, R. F.; Greiner, A.; Lemmer, U.; Bässler, H.; Halliday, D. A.; Bradley, D. D. C.; Burn, P. L.; Holmes, A. B. *J. Phys.: Condens. Matter* **1993**, *5*, 247–260.

(59) Hennebicq, E.; Deleener, C.; Brédas, J. L.; Scholes, G. D.; Beljonne, D. *J. Chem. Phys.* **2006**, *125*, 054901.

(60) *Primary Excitations in Conjugated Polymers: Molecular Exciton versus Semiconductor Band Model*; Sariciftci, N. S., Ed.; World Scientific: Singapore, 1997.

(61) Dykstra, T. E.; Hennebicq, E.; Beljonne, D.; Gierschner, J.; Claudio, G.; Bittner, E. R.; Knoester, J.; Scholes, G. D. *J. Phys. Chem. B* **2009**, *113*, 656–667.

(62) Schweizer, K. S. *J. Chem. Phys.* **1986**, *85*, 1156–1175.

(63) Schreiber, M.; Abe, S. *Synth. Met.* **1993**, *55*, 50–55.

(64) Lhost, O.; Brédas, J. L. *J. Chem. Phys.* **1992**, *96*, 5279–5288.

(65) Galvao, D. S.; Soos, Z. G.; Ramesesha, S.; Etemad, S. *J. Chem. Phys.* **1993**, *98*, 3016–3021.

(66) Soos, Z. G.; Ramasesha, S.; Galvao, D. S.; Etemad, S. *Phys. Rev. B* **1993**, *47*, 1742.

(67) Kohler, B. E.; Samuel, I. D. W. *J. Chem. Phys.* **1995**, *103*, 6248–6252.

(68) Kohler, B. E.; Woehl, J. C. *J. Chem. Phys.* **1995**, *103*, 6253–6256.

(69) Förster, T. *Ann. Physik* **1948**, *437*, 55–75.

(70) Förster, T. *Discuss. Faraday Soc.* **1959**, *27*, 7.

(71) Förster, T. In *Modern Quantum Chemistry: Instambul Lectures. Part III, Action of light and organic Crystals*; Sinanoglu, O., Ed.; Academic Press: New York, 1965; pp 93−137.

(72) Beljonne, D.; Curutchet, C.; Scholes, G. D.; Silbey, R. *J. Phys. Chem. B* **2009**, submitted.

(73) Krueger, B. P.; Scholes, G. D.; Fleming, G. R. *J. Phys. Chem. B* **1998**, *102*, 5378–5386.

(74) Curutchet, C.; Mennucci, B. *J. Am. Chem. Soc.* **2005**, *127*, 16733–16744.

(75) Iozzi, M. F.; Mennucci, B.; Tomasi, J.; Cammi, R. *J. Chem. Phys.* **2004**, *120*, 7029–7040.

(76) Hsu, C. P.; You, Z. Q.; Chen, H. C. H. *J. Phys. Chem. C* **2008**, *112*, 1204–1212.

(77) Fuckel, B.; Kohn, A.; Harding, M. E.; Diezemann, G.; Hinze, G.; Basche, T.; Gauss, J. *J. Chem. Phys.* **2008**, *128*, 074505.

(78) Scholes, G. D.; Curutchet, C.; Mennucci, B.; Cammi, R.; Tomasi, J. *J. Phys. Chem. B* **2007**, *111*, 6978–6982.

(79) Hsu, C. P.; Fleming, G. R.; Head-Gordon, M.; Head-Gordon, T. *J. Chem. Phys.* **2001**, *114*, 3065–3072.

(80) Bodunov, E. N.; Malyshev, V. A. *Fiz. Tverd. Tela* **1979**, *21*, 2717–2723.

(81) Pullerits, T.; Freiberg, A. *Chem. Phys.* **1991**, *149*, 409–418.

(82) Beauregard, M.; Martin, I.; Holzwarth, A. R. *Biochim. Biophys. Acta* **1991**, *1060*, 271–283.

(83) Frenkel, J. *Phys. Z. Sowjetunion* **1936**, *9*, 158.

(84) Frenkel, J. *Phys. Rev.* **1931**, *37*, 1276.

(85) Davydov, A. S. *Theory of molecular excitons*; Plenum Press: New York, 1971.

(86) Kittel, C. *Introduction to solid state physics*; J. Wiley: New York, 1956.

(87) Mc Rae, E. G.; Kasha, M. *J. Chim. Phys.* **1958**, *28*, 721.

(88) Levinson, G. S.; Simpson, W. T.; Curtis, W. *J. Am. Chem. Soc.* **1957**, *79*, 4314–4320.

(89) Heijs, D. J.; Malyshev, V. A.; Knoester, J. *Phys. Rev. Lett.* **2005**, *95*, 177402.

(90) Bednarz, M.; Malyshev, V. A.; Knoester, J. *J. Chem. Phys.* **2002**, *117*, 6200–6213.

(91) Brixner, T.; Stenger, J.; Vaswani, H. M.; Cho, M.; Blankenship, R. E.; Fleming, G. R. *Nature* **2005**, *434*, 625–628.

(92) Klafter, J.; Silbey, R. *Phys. Lett. A* **1980**, *76*, 143–146.

(93) Yang, X.; Dykstra, T. E.; Scholes, G. D. *Phys. Rev. B* **2005**, *71*, 045203.

(94) Yarkony, D.; Silbey, R. *J. Chem. Phys.* **1976**, *65*, 1042–1052.

(95) Yarkony, D. R.; Silbey, R. *J. Chem. Phys.* **1977**, *67*, 5818–5827.

(96) Suarez, A.; Silbey, R.; Oppenheim, I. *J. Chem. Phys.* **1992**, *97*, 5101–5107.

(97) Haken, H.; Strobl, G. *Z. Phys.* **1973**, *262*, 135–148.

(98) Grover, M.; Silbey, R. *J. Chem. Phys.* **1971**, *54*, 4843–4851.

(99) Kapral, R. *Annu. Rev. Phys. Chem.* **2006**, *57*, 129–157.

(100) Zwanzig, R. *J. Chem. Phys.* **1960**, *33*, 1338–1341.

(101) Chernyak, V.; Mukamel, S. *J. Chem. Phys.* **1996**, *105*, 4565–4583.

(102) Cheng, Y. C.; Silbey, R. J. *Phys. Rev. Lett.* **2006**, *96*, 028103.

(103) Jang, S.; Cheng, Y.-C.; Reichman, D. R.; Eaves, J. D. *J. Chem. Phys.* **2008**, *129*, 101104.

(104) Jackson, B.; Silbey, R. *J. Chem. Phys.* **1981**, *75*, 3293–3296.

(105) Schroder, M.; Kleinekathofer, U.; Schreiber, M. *J. Chem. Phys.* **2006**, *124*, 084903.

(106) Leegwater, J. A. *J. Phys. Chem.* **1996**, *100*, 14403–14409.

(107) Mukamel, S. *Principles of Nonlinear Optical Spectroscopy*; Oxford University Press: New York, 1995.

(108) Capek, V.; Barvik, I.; Herman, P. *Chem. Phys.* **2001**, *270*, 141–156.

(109) Cheng, Y. C.; Silbey, R. J. *J. Phys. Chem. B* **2005**, *109*, 21399–21405.

(110) Kubo, R. *Adv. Chem. Phys.* **1969**, *15*, 101–127.

(111) Akimoto, S.; Mimuro, M. *Photochem. Photobiol.* **2007**, *83*, 163–170.

(112) Kennis, J. T. M.; Gobets, B.; van Stokkum, I. H. M.; Dekker, J. P.; van Grondelle, R.; Fleming, G. R. *J. Phys. Chem. B* **2001**, *105*, 4485–4494.

(113) Bradforth, S. E.; Jinenez, R.; Van Mourik, F.; Van Grondelle, R.; Fleming, G. R. *J. Phys. Chem.* **1995**, *99*, 16179–16191.

(114) Marcus, A. H.; Diachun, N. A.; Fayer, M. D. *Macromolecules* **1993**, *26*, 3041–3048.

(115) Gochanour, C. R.; Fayer, M. D. *J. Phys. Chem.* **1981**, *85*, 1989–1994.

(116) Mirkovic, T.; Doust, A. B.; Kim, J.; Wilk, K. E.; Curutchet, C.; Mennucci, B.; Cammi, R.; Curmi, P. M. G.; Scholes, G. D. *Photochem. Photobiol. Sci.* **2007**, *6*, 964–975.

(117) Chang, M. H.; Frampton, M. J.; Anderson, H. L.; Herz, L. M. *Phys. Rev. Lett.* **2007**, *98*, 027402.

(118) Hennebicq, E.; Pourtois, G.; Scholes, G. D.; Herz, L. M.; Russel, D. M.; Silva, C.; Müllen, K.; Brédas, J. L.; Beljonne, D. *J. Am. Chem. Soc.* **2005**, *127*, 4744–4762.

(119) Wells, N. P.; Boudouris, B. W.; Hillmyer, M. A.; Blank, D. A. *J. Phys. Chem. B* **2007**, *111*, 15404–15414.

(120) Ahn, T. S.; Thompson, A. L.; Bharathi, P.; Muller, A.; Bardeen, C. J. *J. Phys. Chem. B* **2006**, *110*, 19810–19819.

(121) McClain, W. M. *J. Chem. Phys.* **1972**, *57*, 2264–2272.

(122) Wagnière, G. *J. Chem. Phys.* **1982**, *76*, 473–480.

(123) Scholes, G. D. *J. Chem. Phys.* **2004**, *121*, 10104–10110.

(124) Andrews, D. L.; Blake, N. P. *J. Phys. A: Math. Gen.* **1989**, *22*, 49–60.

(125) Andrews, D. L.; Thirunamachandran, T. *J. Chem. Phys.* **1977**, *67*, 5026.

(126) Joo, T.; Jia, Y.; Yu, J.-Y.; Lang, M. J.; Fleming, G. R. *J. Chem. Phys.* **1996**, *104*, 6089–6108.

(127) Jonas, D. M.; Lang, M. J.; Nagasawa, Y.; Joo, T.; Fleming, G. R. *J. Phys. Chem.* **1996**, *100*, 12660–12673.

(128) Cho, M. H. *Chem. Rev.* **2008**, *108*, 1331–1418.

(129) Jonas, D. M. *Annu. Rev. Phys. Chem.* **2003**, *54*, 425–463.

(130) Hybl, J. D.; Ferro, A. A.; Jonas, D. M. *J. Chem. Phys.* **2001**, *115*, 6606–6622.

(131) Mukamel, S. *Annu. Rev. Phys. Chem.* **2000**, *51*, 691–729.

(132) Cho, M. H.; Vaswani, H. M.; Brixner, T.; Stenger, J.; Fleming, G. R. *J. Phys. Chem. B* **2005**, *109*, 10542–10556.

(133) Cheng, Y. C.; Engel, G. S.; Fleming, G. R. *Chem. Phys.* **2007**, *341*, 285–295.

(134) Hybl, J. D.; Yu, A.; Farrow, D. A.; Jonas, D. M. *J. Phys. Chem. A* **2002**, *106*, 7651–7654.

(135) Stiopkin, I.; Brixner, T.; Yang, M.; Fleming, G. R. *J. Phys. Chem. B* **2006**, *110*, 20032–20037.

(136) Loparo, J. J.; Roberts, S. T.; Tokmakoff, A. *J. Chem. Phys.* **2006**, *125*, 194521.

(137) Cheng, Y. C.; Fleming, G. R. *J. Phys. Chem. A* **2008**, *112*, 4254–4260.

(138) Kleinekathofer, U. *J. Chem. Phys.* **2004**, *121*, 2505.

(139) Gelin, M. F.; Egorova, D.; Domcke, W. *J. Chem. Phys.* **2005**, *123*, 164112.

(140) Kjellberg, P.; Bruggemann, B.; Pullerits, T. *Phys. Rev. B* **2006**, *74*, 024303.

(141) Salvador, M. R.; Hines, M. A.; Scholes, G. D. *J. Chem. Phys.* **2003**, *118*, 9380.

(142) Kim, J.; Wong, C. Y.; Nair, P. S.; Fritz, K. P.; Kumar, S.; Scholes, G. D. *J. Phys. Chem. B* **2006**, *110*, 25371–25382.

(143) Goodno, G. D.; Dadusc, G.; Miller, R. J. D. *J. Opt. Soc. Am. B* **1998**, *15*, 1791–1794.

(144) Cowan, M. L.; Ogilvie, J. P.; Miller, R. J. D. *Chem. Phys. Lett.* **2004**, *386*, 184–189.

(145) Brixner, T.; Mancal, T.; Stiopkin, I. V.; Fleming, G. R. *J. Chem. Phys.* **2004**, *121*, 4221–4236.

(146) Brixner, T.; Pfeiffer, W.; de Abajo, F. J. G. *Opt. Lett.* **2004**, *29*, 2187–2189.

(147) Gallagher, S. M.; Albrecht, A. W.; Hybl, T. D.; Landin, B. L.; Rajaram, B.; Jonas, D. M. *J. Opt. Soc. Am. B* **1998**, *15*, 2338–2345.

(148) Lepetit, L.; Cheriaux, G.; Joffre, M. *J. Opt. Soc. Am. B* **1995**, *12*, 2467–2474.

(149) Dorrer, C.; Belabas, N.; Likforman, J. P.; Joffre, M. *J. Opt. Soc. Am. B* **2000**, *17*, 1795–1802.

(150) Szymanski, C.; Wu, C. F.; Hooper, J.; Salazar, M. A.; Perdomo, A.; Dukes, A.; McNeill, J. *J. Phys. Chem. B* **2005**, *109*, 8543–8546.

(151) Dubin, F.; Melet, R.; Barisien, T.; Grousson, R.; Legrand, L.; Schott, M.; Voliotis, V. *Nat. Phys.* **2006**, *2*, 32–35.

(152) Claudio, G. C.; Bittner, E. R. *J. Chem. Phys.* **2001**, *115*, 9585.

(153) Claudio, G. C.; Bittner, E. R. *J. Phys. Chem. A* **2003**, *107*, 7092.

(154) Yaliraki, S. N.; Silbey, R. J. *J. Chem. Phys.* **1996**, *104*, 1245–1253.

(155) Cornil, J.; dos Santos, D. A.; Crispins, X.; Silbey, R. J.; Brédas, J. L. *J. Am. Chem. Soc.* **1998**, *120*, 1289–1299.

(156) Karabunarliev, S.; Baumgarten, M.; Müllen, K. *J. Phys. Chem. A* **2000**, *104*, 8236–8243.

(157) Beenken, W. J. D.; Pullerits, T. *J. Phys. Chem. B* **2004**, *108*, 6164–6169.

(158) Liu, L. T.; Yaron, D.; Berg, M. A. *J. Phys. Chem. C* **2007**, *111*, 5770–5782.

(159) Liu, L. T.; Yaron, D.; Sluch, M. I.; Berg, M. A. *J. Phys. Chem. B* **2006**, *110*, 18844–18852.

(160) Wells, N. P.; Blank, D. A. *Phys. Rev. Lett.* **2008**, *100*, 086403.

(161) Scholes, G. D.; Larsen, D. S.; Fleming, G. R.; Rumbles, G.; Burn, P. L. *Phys. Rev. B* **2000**, *61*, 13670.

(162) Beljonne, D.; Pourtois, G.; Silva, C.; Hennebicq, E.; Herz, L. M.; Friend, R. H.; Scholes, G. D.; Setayesh, S.; Müllen, K.; Brédas, J. L. *Proc. Natl. Acad. Sci. U.S.A.* **2002**, *99*, 10982–10987.

(163) Dykstra, T. E.; Kovalevskij, V.; Yang, X.; Scholes, G. D. *Chem. Phys.* **2005**, *318*, 21–32.

(164) Schwartz, B. J. *Annu. Rev. Phys. Chem.* **2003**, *54*, 141–72.

(165) Sumpter, B. G.; Kumar, P.; Mehta, A.; Barnes, M. D.; Shelton, W. A.; Harrison, R. J. *J. Phys. Chem. B* **2005**, *109*, 7671–7685.

(166) Huser, T.; Yan, M.; Rothberg, L. J. *Proc. Natl. Acad. Sci. U.S.A.* **2000**, *97*, 11187–11191.

(167) Yu, J.; Hu, D.; Barbara, P. F. *Science* **2000**, *289*, 1327–1330.

(168) Nguyen, T.-Q.; Wu, J.; Tolbert, S. H.; Schwartz, B. J. *Adv. Mater.* **2001**, *13*, 609.

(169) Nguyen, T. Q.; Wu, J. J.; Doan, V.; Schwartz, B. J.; Tolbert, S. H. *Science* **2000**, *288*, 652–656.

(170) Collison, C. J.; Rothberg, L. J.; Treemaneekarn, V.; Li, Y. *Macromolecules* **2001**, *34*, 2346–2352.

(171) Sperling, J.; Nemeth, A.; Baum, P.; Sanda, F.; Riedle, E.; Kauffmann, H. F.; Mukamel, S.; Milota, F. *Chem. Phys.* **2008**, *349*, 244–249.

(172) Wu, C. F.; Peng, H. S.; Jiang, Y. F.; McNeill, J. *J. Phys. Chem. B* **2006**, *110*, 14148–14154.

(173) Wu, C. F.; Szymanski, C.; Cain, Z.; McNeill, J. *J. Am. Chem. Soc.* **2007**, *129*, 12904.

(174) Wu, C. F.; Zheng, Y. L.; Szymanski, C.; McNeill, J. *J. Phys. Chem. C* **2008**, *112*, 1772–1781.

(175) Wu, C. F.; Szymanski, C.; McNeill, J. *Langmuir* **2006**, *22*, 2956–2960.

(176) Padmanaban, G.; Ramakrishnan, S. *J. Am. Chem. Soc.* **2000**, *122*, 2244–2251.

(177) Traiphol, R.; Charoenthai, N. *Synth. Met.* **2008**, *158*, 135–142.

(178) Nguyen, T.-Q.; Doan, V.; Schwartz, B. J. *J. Chem. Phys.* **1999**, *110*, 4068.

(179) Traiphol, R.; Charoenthai, N.; Srikhirin, T.; Kerdeharoen, T.; Osotchan, T.; Maturos, T. *Polymer* **2007**, *48*, 813–826.

(180) Traiphol, R.; Charoenthai, N. *Macromol. Res.* **2008**, *16*, 224–230.

(181) Padmanaban, G.; Ramakrishnan, S. *J. Phys. Chem. B* **2004**, *108*, 14933–14941.

(182) Martini, I. B.; Smith, A. D.; Schwartz, B. J. *Phys. Rev. B* **2004**, *69*, 035204.

(183) Grage, M. M. L.; Wood, P. W.; Ruseckas, A.; Pullerits, T.; Mitchell, W.; Burn, P. L.; Samuel, I. D. W.; Sundstrom, V. *J. Chem. Phys.* **2003**, *118*, 7644–7650.

(184) Grage, M. M. L.; Zaushitsyn, Y.; Yartsev, A.; Chachisvilis, M.; Sundstrom, V.; Pullerits, T. *Phys. Rev. B* **2003**, *67*, 205207.

(185) Chang, R.; Hayashi, M.; Lin, S. H.; Hsu, J.-H.; Fann, W. S. *J. Chem. Phys.* **2001**, *115*, 4339–4348.

(186) Herz, L. M.; Silva, C.; Grimsdale, A. C.; Müllen, K.; Phillips, R. T. *Phys. Rev. B* **2004**, *70*, 165207.

(187) Vaughan, H. L.; Dias, F. M. B.; Monkman, A. P. *J. Chem. Phys.* **2005**, *122*, 014902.

(188) Ruseckas, A.; Samuel, I. D. W. *Phys. Status Solidi C* **2006**, *3*, 263–266.

(189) Didraga, C.; Malyshev, V. A.; Knoester, J. *J. Phys. Chem. B* **2006**, *110*, 18818–18827.

(190) Zheng, G.; Clark, S. J.; Tulip, P. R.; Brand, S.; Abram, R. A. *J. Chem. Phys.* **2005**, *123*, 024904.

(191) Capaz, R. B.; Caldas, M. J. *Phys. Rev. B* **2003**, *67*, 205205.

(192) Orion, I.; Buisson, J. P.; Lefrant, S. *Phys. Rev. B* **1998**, *57*, 7050–7065.

(193) Tian, B.; Zerbi, G.; Mullen, K. *J. Chem. Phys.* **1991**, *95*, 3198–3207.

(194) Sakamoto, A.; Furukawa, Y.; Tasumi, M. *J. Phys. Chem.* **1992**, *96*, 1490–1494.

(195) Fleming, G. R. *Chemical applications of ultrafast spectroscopy*; Oxford University Press: New York 1986; Vol. 13.

(196) Zewail, A. H. *J. Phys. Chem.* **1996**, *100*, 12701–12724.

(197) Dantus, M. *Annu. Rev. Phys. Chem.* **2001**, *52*, 639.

(198) Grimberg, B. I.; Lozovoy, V. V.; Dantus, M.; Mukamel, S. *J. Phys. Chem. A* **2002**, *106*, 697–718.

(199) Lozovoy, V. V.; Grimberg, B. I.; Pastirk, I.; Dantus, M. *Chem. Phys.* **2001**, *267*, 99–114.

(200) Nagasawa, Y.; Mori, Y.; Nakagawa, Y.; Miyasuka, H.; Okada, T. *J. Phys. Chem. B* **2005**, *109*, 11946–11952.

(201) Bardeen, C. J.; Shank, C. V. *Chem. Phys. Lett.* **1993**, *203*, 535–539.

(202) Arnett, D. C.; Moser, C. C.; Dutton, P. L.; Scherer, N. F. *J. Phys. Chem. B* **1999**, *103*, 2014–2032.

(203) Wynne, K.; Hochstrasser, R. M. *Chem. Phys.* **1993**, *171*, 179–188.

(204) Cina, J. A.; Fleming, G. R. *J. Phys. Chem. A* **2004**, *108*, 11196–11208.

(205) Farrow, D. A.; Qian, W.; Smith, E. R.; Ferro, A. A.; Jonas, D. M. *J. Chem. Phys.* **2008**, *128*, 144510.

(206) Smith, E.; Farrow, D.; Jonas, D. *J. Chem. Phys.* **2005**, *123*, 044102.

(207) Kilin, D. S.; Pereversev, Y. V.; Prezhdo, O. V. *J. Chem. Phys.* **2004**, *120*, 11209–11223.

(208) Bakalis, L. D.; Knoester, J. *J. Phys. Chem. B* **1999**, *103*, 6620–6628.

(209) Durrant, J. R.; Knoester, J.; Wiersma, D. A. *Chem. Phys. Lett.* **1994**, *222*, 450–456.

(210) Fidder, H.; Knoester, J.; Wiersma, D. A. *J. Chem. Phys.* **1993**, *98*, 6564–6566.

(211) Heijs, D. J.; Dijkstra, A. G.; Knoester, *J. Chem. Phys.* **2007**, *341*, 230–239.

(212) Johnson, A. E.; Kumazaki, S.; Yoshihara, K. *Chem. Phys. Lett.* **1993**, *211*, 511–515.

(213) Gulbinas, V.; Mineviciute, I.; Hertel, D.; Wellander, R.; Yartsev, A.; Sundstrom, V. *J. Chem. Phys.* **2007**, *127*, 144907.

(214) Miranda, P. B.; Moses, D.; Heeger, A. J. *Phys. Rev. B* **2004**, *70*, 085212.

(215) Hendry, E.; Schins, J. M.; Candeias, L. P.; Siebbeles, L. D. A.; Bonn, M. *Phys. Rev. Lett.* **2004**, *92*, 196601.

(216) Sheng, C. X.; Tong, M.; Singh, S.; Vardeny, Z. V. *Phys. Rev. B* **2007**, *75*, 085206.

(217) Greenham, N. C.; Samuel, I. D. W.; Hayes, G. R.; Phillips, R. T.; Kessener, Y. A. R. R.; Moratti, S. C.; Holmes, A. B.; Friend, R. H. *Chem. Phys. Lett.* **1995**, *241*, 89–96.

(218) Singh, S.; Drori, T.; Vardeny, Z. V. *Phys. Rev. B* **2008**, *77*, 195304.

(219) Scholes, G. D.; Harcourt, R. D.; Ghiggino, K. P. *J. Chem. Phys.* **1995**, *102*, 9574–9581.

(220) Harcourt, R. D.; Scholes, G. D.; Ghiggino, K. P. *J. Chem. Phys.* **1994**, *101*, 10521–10525.

(221) Cheng, Y. C.; Lee, H.; Fleming, G. R. *J. Phys. Chem. A* **2007**, *111*, 9499–9508.

(222) Egorova, D. *Chem. Phys.* **2008**, *347*, 166–176.

(223) Plenio, M. B.; Huelga, S. F. *New J. Phys* **2008**, *10*, 113019.

(224) Mohseni, M.; Rebentrost, P.; Lloyd, P.; Aspuru-Guzik, A. *J. Chem. Phys.* **2008**, *129*, 174106.

(225) Lee, H.; Cheng, Y. C.; Fleming, G. R. *Science* **2007**, *316*, 1462–1465.

(226) Laird, B. B.; Skinner, J. L. *J. Chem. Phys.* **94**, *94*, 4405.

(227) Dunkel, E. R.; Bonella, S.; Coker, D. F. *J. Chem. Phys.* **2008**, *129*, 114106.

(228) Lee, S.-Y.; Heller, E. J. *J. Chem. Phys.* **1979**, *71*, 4777–4788.

(229) Myers Kelley, A. *J. Phys. Chem. A* **2008**, *112*, 11975–11991.

JP810757X